# Evolution of a black ring by Hawking evaporation

Mitsuhiro Matsumoto

## ABSTRACT

Black objects lose their mass and angular momenta through evaporation by Hawking radiation, and the investigation of their time evolution has a long history. In this thesis, after reviewing previous studies on the time evolution of evaporating black holes, we study this problem for a five-dimensional doubly spinning black ring. We consider a thin black ring with a small thickness parameter, $\lambda \ll 1$, which can be approximated by a boosted Kerr string locally. For simplicity, we concentrate on the case in which the black objects emit only massless scalar particles. We show that a thin black ring evaporates with fixing its thickness parameter $\lambda$. Further, in the case of an Emparan-Reall black ring, we derive analytic formulas for the time evolution, which has one parameter to be evaluated numerically. By developing a numerical code, we determine the value of this parameter with sufficient numerical accuracy. We demonstrate that the lifetime of a thin black ring is shorter by a factor of $O(\lambda^2)$ compared to a five-dimensional Schwarzschild black hole with the same initial mass. We also evaluate the energy and angular spectra of radiated particles in the evaporation of a thin Emparan-Reall black ring. In addition to the evaporation of a thin black ring approximated by a boosted black string, we also discuss evaporation of a thin five-dimensional unboosted Schwarzschild black string whose Schwarzschild radius $2M_K$ is much smaller than the compactification scale $L$ along the string direction. We study the time evolution of its mass and the energy spectrum of emitted particle from the black string, and compare them with those of a four-dimensional Schwarzschild black hole. We show that the energy emission rate of a black string is larger by a factor of $O(L/M_K)$ compared to that of a black hole.

# Contents

# 1 Introduction

In four spacetime dimensions, a stationary, asymptotically flat, vacuum black hole is completely characterized by its mass and spin angular momentum[1]. In particular, the topology of its event horizon must be a sphere [2]. By contrast, in five dimensions, in addition to the Myers-Perry black hole [3] which is a natural generalization of the four-dimensional Kerr black hole, various exact solutions of black objects with nonspherical horizon topologies have been found [4, 5, 6, 7, 8](see [9] for a review). In this thesis, we focus attention to black ring solutions with the $S^1 \times S^2$ horizon topology. A black ring solution rotating in the direction of $S^1$ was found by Emparan and Reall [4]. Since a five-dimensional spacetime can have two angular momenta, Pomeransky and Sen'kov [10] extended it to a solution with two independent rotation parameters (i.e., spinning both in the directions of $S^1$ and $S^2$).

A black hole is known to evaporate due to quantum effects of fields in curved spacetime as shown by Hawking [11]. The rate of mass and angular momentum loss by the Hawking radiation for a Kerr black hole was first studied by Page [12, 13] taking account of fields with spins 1/2, 1, and 2, and it was shown that a Kerr black hole spins down to a nonrotating black hole regardless of its initial state. However, Chambers *et al.* [14] (see also [15]) showed that if only a massless scalar field is taken into account (i.e., in the absence of fields with nonzero spin), a four-dimensional Kerr black hole evolves to a state with the nonvanishing nondimensional rotation parameter, $a/M \simeq 0.555$. This analysis was extended to five-dimensional Myers-Perry black holes by Nomura *et al* [16]. They showed that any such black hole with nonzero rotation parameters $a$ and $b$ evolves toward an asymptotic state with $a/M^{1/2} = b/M^{1/2} \simeq 0.1975(8/3\pi)^{1/2}$. Here, this value is independent of the initial values of $a$ and $b$.

It is interesting to extend these studies to the case of a black ring. Although the Hawking radiation of black rings has been studied in various context [17, 18, 19, 20], the time evolution of a black ring has not been studied up to now. The difficulty in this study is that the method of mode decomposition of the Klein-Gordon field in this spacetime is not known since separation of variables has not been realized, and therefore, two-dimensional numerical calculations of eigenfunctions are required. In order to avoid this difficulty, we consider a thin black ring with a small thickness parameter, $\lambda \ll 1$. Here, "thin" or the small thickness parameter $\lambda$ means that the $S^2$ radius is much smaller compared to the $S^1$ radius. In such a situation, a black ring can be approximated by a boosted black string. Then, the separation of variables for the scalar field can be done, and we have well defined modes.

Using this thin-limit approximation, we give a formulation to study the evolution of a thin Pomeransky-Sen'kov black ring by the Hawking radiation, and discuss general features that do not depend on details of the greybody factor. Then, we apply our method to a special case of the Emparan-Reall black ring without $S^2$ rotation, and derive a semi-analytic formula for the time evolution of the evaporation. Here, the formula is semi-analytic in the sense that the evolution is expressed by analytic formulas but they include one parameter

related to the greybody factors that have to be evaluated numerically. By developing a numerical code, we also determine the value of this parameter with sufficient numerical accuracy.

In addition to the time evolution, we present numerical results on detailed properties of the evaporation of a thin Emparan-Reall black ring. Specifically, we examine the energy and angular spectra of emitted particles in the evaporation. In order to clarify the property of the energy spectrum that is specific to the evaporation of a black ring, we discuss the results by comparing it with that of a four-dimensional Schwarzschild black hole.

Because a black ring was approximated by a black string in the thin-limit approximation above, we can apply our method also to evaporation of a thin black string. For this reason, we discuss evaporation of a thin Schwarzschild black string in the unboosted frame. Here, a thin black string means that the Schwarzschild radius $2M_K$ is much smaller than the compactification scale $L$ along the string direction. In addition to the formulas for time evolution, we present numerical results on detailed properties of evaporation such as an energy spectrum and compare them with those of a four-dimensional Schwarzschild black hole. We also discuss the connection of these results with the evaporation of a thin black ring.

This thesis is organized as follows. In Sec. 2, we review the evolution of a four-dimensional Kerr black hole and a five-dimensional Myers-Perry black hole. In Sec. 3, the black ring solution is reviewed and its boosted Kerr string limit is shown. In Sec. 4, we derive the equations that determine the emission rates of mass and angular momenta of a black ring via Hawking radiation. In Sec. 5, the time evolution of evaporating black rings is discussed and we check the validity of our numerical result by studying the DeWitt approximation. In Sec. 6, we present the energy and angular spectrum of emitted particles in the evaporation of a thin Emparan-Reall black ring. In addition, we discuss evaporation of a thin Schwarzschild black string. Sec. 7 is devoted to a conclusion. To simplify the notation, we use the natural units $\hbar = c = k_B = 1$.

# 2 Evolution of evaporating spherical black holes

In this section, we review the evolution of black holes with spherical horizon by Hawking evaporation. In the first subsection, we explain Hawking radiation. In the remaining two subsections, the time evolution of a Kerr black hole and a Myers-Perry black hole, emitting massless scalar particles, is discussed.

## 2.1 Hawking radiation

Black holes do not only absorb matter around them, but also emit radiation with a thermal spectrum due to quantum effects, which is called *Hawking radiation*. We derive the thermal spectrum, following the discussion in Ford's lecture note[21].

### 2.1.1 Particle creation

We consider a massless scalar field satisfying the Klein-Gordon equation in curved spacetime

$$(-g)^{-1/2}\,\partial_\mu\left(\sqrt{-g}g^{\mu\nu}\partial_\nu\Phi\right)=0, \tag{2.1}$$

where $g$ is the determinant of the metric $g_{\mu\nu}$. We define the inner product of a pair of solutions of the Klein-Gordon equation by

$$(f_1,f_2)=i\int(f_2^*\partial_\mu f_1-f_1\partial_\mu f_2^*)d\Sigma^\mu, \tag{2.2}$$

where $d\Sigma^\mu = d\Sigma\, n^\mu$. Here, $d\Sigma$ is the volume element in a given spacelike hypersurface, and $n^\mu$ is the timelike unit vector normal to this hypersurface.

Let $\{f_j, f_j^*\}$ be a complete set of solutions of Eq. (2.1), where $f_j$ has a positive norm. We write the field $\Phi$ using annihilation and creation operators $a_j$ and $a_{j'}^\dagger$ as

$$\Phi=\sum_j(a_j f_j+a_j^\dagger f_j^*). \tag{2.3}$$

The commutation relation is $[a_j, a_{j'}^\dagger]=\delta_{jj'}$ and a vacuum state $|0\rangle$ is defined by $a_j|0\rangle=0$.

Let us consider a spacetime which is asymptotically flat in the past and in the future, but which is non-flat in the intermediate region. Let $\{f_j\}$ be positive frequency solutions in the past (the "in-region"), and let $\{F_j\}$ be positive frequency solutions in the future (the "out-region"). These modes are orthonormal in the sense that

$$(f_j,f_{j'})=(F_j,F_{j'})=\delta_{jj'},\qquad (f_j^*,f_{j'}^*)=(F_j^*,F_{j'}^*)=-\delta_{jj'}, \tag{2.4}$$

with all other inner products vanishing. We expand the in-modes in terms of the out-modes:

$$f_j=\sum_k(\alpha_{jk}F_k+\beta_{jk}F_k^*). \tag{2.5}$$

From Eq. (2.4), we have the conditions for $\alpha_{jk}$ and $\beta_{jk}$.

$$\sum_k (\alpha_{jk}\alpha^*_{j'k} - \beta_{jk}\beta^*_{j'k}) = \delta_{jj'}, \qquad \sum_k (\alpha_{jk}\alpha_{j'k} - \beta_{jk}\beta_{j'k}) = 0. \tag{2.6}$$

The inverse expansion is

$$F_k = \sum_j (\alpha^*_{jk} f_j - \beta_{jk} f^*_j). \tag{2.7}$$

The field $\Phi$ can be also expanded in terms of $\{F_j\}$.

$$\Phi = \sum_j (b_j F_j + b^\dagger_j F^*_j). \tag{2.8}$$

The $a_j$ and $a^\dagger_j$ are annihilation and creation operators, respectively, in the in-region. On the other hand, the $b_j$ and $b^\dagger_j$ are the corresponding operators for the out-region. The in-vacuum state is defined by $a_j|0\rangle_{in} = 0$, whereas the out-vacuum state is defined by $b_j|0\rangle_{out} = 0$. These creation and annihilation operators are related to each other:

$$a_j = \sum_k (\alpha^*_{jk} b_k - \beta^*_{jk} b^\dagger_k), \qquad b_k = \sum_j (\alpha_{jk} a_j + \beta^*_{jk} a^\dagger_j). \tag{2.9}$$

This relation is called a Bogolubov transformation, and the $\alpha_{jk}$ and $\beta_{jk}$ are called the Bogolubov coefficients.

In the following, we will consider the gravitational collapse. Namely, the in-region is described by the past null infinity $\mathcal{I}^-$, and the out-region is described by the future null infinity $\mathcal{I}^+$ and the future event horizon $\mathcal{H}^+$. The number operator which counts particles on $\mathcal{I}^+$ is $N_\ell = b^\dagger_\ell b_\ell$, where $\ell$ is the mode which left $\mathcal{I}^-$ and reached $\mathcal{I}^+$, not $\mathcal{H}^+$. Thus the mean number of particles created into mode $\ell$ is

$$\langle N_\ell \rangle = {}_{in}\langle 0|b^\dagger_\ell b_\ell|0\rangle_{in} = \sum_j |\beta_{j\ell}|^2. \tag{2.10}$$

If any of the $\beta_{j\ell}$ coefficients are non-zero, the particle creation occurs.

### 2.1.2 Thermal spectrum

For simplicity, we wil concentrate on the case of a massless scalar field in a four-dimensional nonrotating black hole, i.e., a Schwarzschild black hole. The metric of a Schwarzschild black hole is given by

$$ds^2 = -f(r)dt^2 + \frac{dr^2}{f(r)} + r^2 d\Omega^2, \tag{2.11}$$

where

$$f(r) = 1 - \frac{2G_4 M_S}{r}, \qquad d\Omega^2 = d\theta^2 + \sin^2\theta d\phi^2. \tag{2.12}$$

Here, $G_4$ is the four-dimensional gravitational constant and $M_S$ is the mass of the Schwarzschild black hole. Its event horizon is located at $r = 2G_4M_S$. For later use, we define the advanced and retarded time coordinates as

$$v = t + r^*, \qquad u = t - r^*, \tag{2.13}$$

where $r^*$ is the tortoise coordinate given by

$$r^* = r + 2G_4M_S \ln\left(\frac{r - 2G_4M_S}{2G_4M_S}\right). \tag{2.14}$$

We imagine that the black hole was formed at some time in the past by gravitational collapse, and assume that no scalar particles were present before the collapse began. The in-modes, $f_{\omega\ell m}$, are pure positive frequency on the past null infinity $\mathcal{I}^-$, so $f_{\omega\ell m} \sim e^{-i\omega v}$ as $v \to -\infty$, Similarly, the out-modes, $F_{\omega\ell m}$, are pure positive frequency on the future null infinity $\mathcal{I}^+$, so $F_{\omega\ell m} \sim e^{-i\omega u}$ as $u \to \infty$. In order to determine the particle creation, we need to calculate the Bogolubov coefficients.

In WKB approximation, the out-modes asymptotically behave as

$$F_{\omega\ell m} \sim \frac{Y_{\ell m}(\theta,\phi)}{\sqrt{4\pi\omega}\, r} \times \begin{cases} e^{-i\omega u}, & \text{on } \mathcal{I}^+ \\ A(\omega) e^{4G_4M_S i\omega \ln[(v_0 - v)/C]}, & \text{on } \mathcal{I}^- \end{cases} \tag{2.15}$$

where $Y_{\ell m}(\theta,\phi)$ is a spherical harmonic, $C$ is a constant, and $v_0$ is the limiting value of $v$ for rays which pass through the body before the horizon forms. Therefore, the out-modes on $\mathcal{I}^-$ have the form

$$F_{\omega\ell m} \sim \begin{cases} A(\omega) e^{4G_4M_S i\omega \ln[(v_0 - v)/C]}, & v < v_0 \\ 0, & v > v_0 \end{cases} \tag{2.16}$$

We expand out-modes in terms of in-modes:

$$F_{\omega\ell m} = \int_0^\infty d\omega' \Big(\alpha^*_{\omega'\omega} f_{\omega'\ell m} - \beta_{\omega'\omega} f^*_{\omega'\ell m}\Big). \tag{2.17}$$

Here we did not write the common modes $(\ell, m)$ of the Bogolubov coefficients $\alpha^*_{\omega'\ell m,\omega\ell m}$ and $\beta_{\omega'\ell m,\omega\ell m}$. Thus, $\beta_{\omega'\omega}$ is

$$\begin{aligned} \beta_{\omega'\omega} &= -\frac{1}{2\pi}\sqrt{\frac{\omega'}{\omega}} A(\omega) \int_{-\infty}^{v_0} dv\, e^{-i\omega' v} e^{4G_4M_S i\omega \ln[(v_0 - v)/C]} \\ &= -\frac{1}{2\pi}\sqrt{\frac{\omega'}{\omega}} A(\omega) e^{i\omega v_0} \int_0^\infty dv' e^{i\omega' v'} e^{4G_4M_S i\omega \ln(v'/C)}, \end{aligned} \tag{2.18}$$

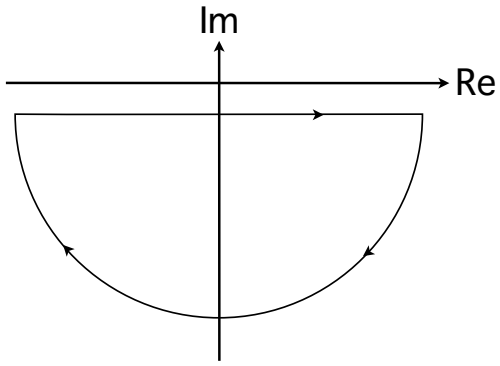


Figure 1: The closed contour of the integration in Eq. (2.20).

where $v' = v_0 - v$. On the other hand, $\alpha^*_{\omega'\omega}$ is

$$\begin{aligned}\alpha^*_{\omega'\omega} &= \frac{1}{2\pi}\sqrt{\frac{\omega'}{\omega}}A(\omega)\int_{-\infty}^{v_0} dv\, e^{i\omega' v} e^{4G_4 M_S i\omega \ln[(v_0-v)/C]} \\ &= \frac{1}{2\pi}\sqrt{\frac{\omega'}{\omega}}A(\omega)e^{i\omega v_0}\int_0^{\infty} dv' e^{-i\omega' v'} e^{4G_4 M_S i\omega \ln(v'/C)} \\ &= -\frac{1}{2\pi}\sqrt{\frac{\omega'}{\omega}}A(\omega)e^{i\omega v_0} e^{4\pi G_4 M_S \omega}\int_0^{\infty} dv' e^{i\omega' v'} e^{4G_4 M_S i\omega \ln(v'/C)}.\end{aligned} \tag{2.19}$$

Here, we use

$$\oint_C dv'\, e^{-i\omega' v'}\, e^{4G_4 M_S i\omega\, \ln(v'/C)} = 0, \tag{2.20}$$

where the integration is taken around the closed contour $C$ illustrated in Fig. 1. From Eq. (2.18) and Eq. (2.19), the Bogolubov coefficients are related to each other as

$$|\alpha_{\omega'\omega}| = e^{4\pi G_4 M_S \omega}|\beta_{\omega'\omega}|. \tag{2.21}$$

The condition on the Bogolubov coefficients, Eq. (2.6), is written as

$$\sum_{\omega'}\Big(|\alpha_{\omega'\omega}|^2 - |\beta_{\omega'\omega}|^2\Big) = \sum_{\omega'}\Big(e^{8\pi G_4 M_S\omega} - 1\Big)|\beta_{\omega'\omega}|^2 = 1. \tag{2.22}$$

The mean number of particles created into mode $(\omega, \ell, m)$ is now given by

$$\langle N_{\omega,\ell,m}\rangle = \sum_{\omega'}|\beta_{\omega'\omega}|^2 = \frac{1}{e^{8\pi G_4 M_S\omega} - 1}. \tag{2.23}$$

This is a thermal spectrum with a temperature of

$$T_S = \frac{1}{8\pi G_4 M_S} \tag{2.24}$$

which is the Hawking temperature of the black hole.

This discussion can be extended to the case of $D(> 4)$ dimensional nonrotating spherical black holes. The difference is that instead of $\omega$ and $T_S$, we need to use the energy of a scalar particle in the background of a D-dimensional nonrotating spherical black hole and the temperature of the horizon. In the rotating case, we have to replace $\omega$ by the energy $\omega_*$ of the mode with respect to the null geodesic generator of the black hole horizons because the mode function behaves as $\exp(-i\omega_* u_\pm)$ in the coordinates that are regular around the black hole horizon, where $u_\pm$ is the advanced time/retarded time around the horizon. In general, this null geodesic generator $\xi$ can be written as $\xi = \partial_t + \sum_j \Omega_j \partial_{\phi^j}$ in terms of the time translation Killing vector $\partial_t$ and the rotational Killing vectors $\partial_{\phi^j}$. From this, it follows that $\omega_*$ for the mode $\propto \exp(-i\omega t + i\sum_j m_j \phi^j)$ is expressed as

$$\omega_* = \omega - \sum_j m^j \Omega_j. \tag{2.25}$$

### 2.1.3 Greybody factor

Particles emitted from a black hole traverse a curved spacetime geometry before they reach an observer located at infinity. The black hole background thus work as a potential barrier for them and give a deviation from the blackbody radiation. Though particles emitted with sufficiently high energy reach the observer, particle emitted with law energy go back to the black hole by its gravitational pull. Therefore, the accurate expected number of particles emitted per unit time for each mode for a Schwarzschild black hole is given by

$$\langle N_S \rangle = \frac{\Gamma^{(\mathrm{Sch})}_{\ell m}(\omega)}{e^{\omega/T_S} - 1}, \tag{2.26}$$

where $\Gamma^{(\mathrm{Sch})}_{\ell m}(\omega)$ is a deviation from the blackbody radiation, called *greybody factor*. The greybody factor is the probability for an outgoing wave of the corresponding modes to reach infinity. Owing to the flux conservation, this coincides with the absorption probability of the incoming wave of the corresponding modes.

Next, we formulate the time evolution of the black hole mass. Particles emitted in a time interval $\Delta t$ have the following discrete energy:

$$\Delta\omega = \frac{2\pi}{\Delta t} \times (\text{natural number}). \tag{2.27}$$

The energy of the particles emitted in $\Delta t$ for each mode is therefore

$$\frac{\Delta E}{\Delta t} = \frac{\Delta\omega}{2\pi}\omega\langle N_S \rangle. \tag{2.28}$$

Because the total energy can be obtained if we take summation of Eq. (2.28) over all modes, the emission rate of the mass of the black hole is formulated as

$$-\frac{dM_S}{dt} = \frac{1}{2\pi}\sum_{\ell m}\int_0^\infty \omega\langle N_S\rangle d\omega, \tag{2.29}$$

where the summation is taken over all modes. In order to determine the time evolution of a black hole in Hawing radiation, we need to obtain the greybody factor for each mode, which has to be evaluated numerically.

## 2.2 Evolution of a evaporating Kerr black hole

We discuss the evolution of a Kerr black hole emitting scalar radiation via the Hawking process [14] (see also [15]) .

### 2.2.1 Kerr solution

The metric of a Kerr black hole is given in the Boyer-Lindquist coordinates as

$$\begin{aligned} ds^2 =& -\left(1-\frac{2G_4M_Kr}{\rho^2}\right)dt^2 - \frac{2G_4M_Kar\sin^2\theta}{\rho^2}\left(dtd\phi + d\phi dt\right) \\ &+ \frac{\rho^2}{\Delta}dr^2 + \rho^2 d\theta^2 + \frac{\sin^2\theta}{\rho^2}\left[\left(r^2+a^2\right)^2 - a^2\Delta\sin^2\theta\right]d\phi^2, \end{aligned} \tag{2.30}$$

where $\rho^2 = r^2 + a^2\cos^2\theta$ and $\Delta = r^2 - 2G_4M_Kr + a^2$. $M_K$ and $a$ correspond to the mass and rotational parameter, respectively. One can recover the Schwarzschild metric (2.11) by setting $a = 0$. The event horizon is located at $r = r_+$ where

$$r_\pm := G_4M_K \pm \sqrt{G_4M_K^2 - a^2} = G_4M_K(1 \pm \sqrt{1-a_*^2}), \tag{2.31}$$

with $a_* := a/(G_4M_K)$. The temperature and surface gravity of the horizon are

$$T_K = \frac{\kappa_K}{2\pi}, \qquad \kappa_K = \frac{r_+ - r_-}{4G_4M_Kr_+}. \tag{2.32}$$

We transform the Boyer-Lindquist coordinates (2.30) to the Kerr ingoing coordinates $(v, r, \theta, \tilde{\phi})$. Here, $(v, \tilde{\phi})$ are introduced as

$$dv = dt + (r^2+a^2)\frac{dr}{\Delta}, \qquad d\tilde{\phi} = d\phi + a\frac{dr}{\Delta}. \tag{2.33}$$

With these coordinates, the Kerr metric in the Kerr ingoing coordinates is given by

$$\begin{aligned} ds^2 =& -\left(1-\frac{2G_4M_Kr}{\rho^2}\right)dv^2 - \frac{2G_4M_Kar\sin^2\theta}{\rho^2}\left(d\tilde{\phi}dv + dvd\tilde{\phi}\right) \\ &- 2a\sin^2\theta d\tilde{\phi}dr + 2drdv + \rho^2 d\theta^2 \\ &+ \frac{\sin^2\theta}{\rho^2}\left[\left(r^2+a^2\right)^2 - a^2\Delta\sin^2\theta\right]d\tilde{\phi}^2 \end{aligned} \tag{2.34}$$

### 2.2.2 Formulation

We formulate the emission rate of the mass and angular momentum of the Kerr black hole, following Page[13].

In terms of Kerr-ingoing coordinates $(v, r, \theta, \tilde{\phi})$, the Klein-Gordon equation $\Box\phi = 0$, separates by writing $\phi = R(r)S(\theta)e^{-i\omega v}e^{im\tilde{\phi}}$, where the angular function $S(\theta)$ is a spheroidal harmonics. The radial function, $R(r)$, satisfies

$$\left[\frac{d}{dr}\Delta\frac{d}{dr} - 2iK\frac{d}{dr} - 2i\omega r - \lambda\right] R(r) = 0, \tag{2.35}$$

where $K = (r^2 + a^2)\omega - am$, $\lambda = E_{\ell m\omega} - 2am\omega + a^2\omega^2$, and $E_{\ell m\omega}$ is the separation constant. Asymptotic solutions can be expressed by

$$R \longrightarrow \begin{cases} Z_{\rm hole} & r \to r_+, \\ Z_{\rm in}r^{-1} + Z_{\rm out}r^{-1}e^{2i\omega r} & r \to \infty. \end{cases} \tag{2.36}$$

The subscript "in" refers to an ingoing wave originating from infinity, "out" refers to an outgoing wave reflected from the black hole that propagates toward infinity, and "hole" refers to the component of the wave that is transmitted into the black hole through the horizon at $r = r_+$. The greybody factor $\Gamma^{(\rm Kerr)}_{\ell m}(\omega)$ is

$$\Gamma^{(\rm Kerr)}_{\ell m}(\omega) = 1 - \left|\frac{Z_{\rm out}}{Z_{\rm in}}\right|^2. \tag{2.37}$$

We express the rates at which the mass and angular momentum decrease by the quantities

$$f := -M_K^2\dot{M}_K, \qquad g := -\frac{M_K}{a_*}\dot{J}_K. \tag{2.38}$$

where the dot ( $\dot{}$ ) denotes the derivative with respect to $t$. This definitions remove overall dependence on the size (mass) of the black hole. The coordinate $t$ is the usual Boyer-Lindquist time coordinate. These quantities will determine the evolution of the Kerr black hole, which is defined by

$$\begin{pmatrix} f \\ g \end{pmatrix} = \sum_{l,m}\frac{1}{2\pi}\int_0^\infty dx \frac{\Gamma^{(\rm Kerr)}_{\ell m}(\omega)}{e^{(\omega - m\Omega_K)/T_K} - 1}\begin{pmatrix} x \\ ma_*^{-1} \end{pmatrix}. \tag{2.39}$$

Here $\Omega_K = a_*/2r_+$ is the surface angular frequency, and we have defined $x = M_K\omega$. The relative magnitude of the mass and angular momentum loss rates will determine whether or not the black hole will spin down to a nonzero value of $a_*$. To obtain the evolution of $a_*$, we differentiate $a_* = J_K/M_K^2$ with respect to time $t$. From Eq. (2.38), the equation for $a_*$ is derived as

$$\frac{\dot{a}_*}{a_*} = -\frac{hf}{M_K^3}, \tag{2.40}$$

where $h(a_*)$ was defined by

$$h(a_*) := \frac{g(a_*)}{f(a_*)} - 2. \tag{2.41}$$

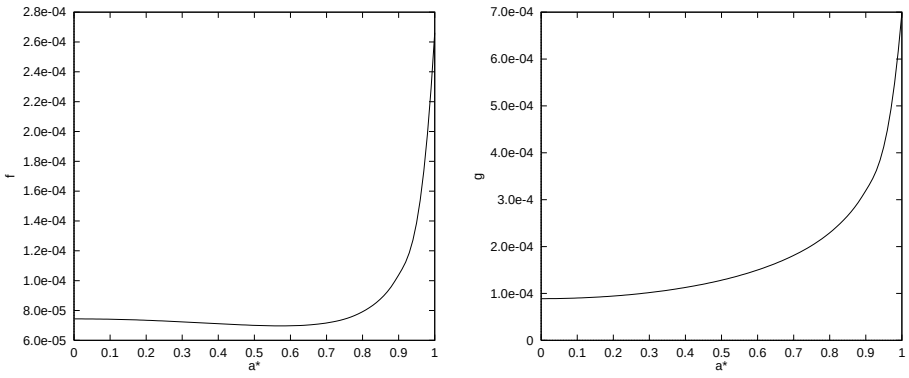


Figure 2: The scale invariant mass(left panel) and angular momentum(right panel) loss rates, due to scalar particle emission, for a Kerr black hole. In the left panel, the mass loss rate approaches the value $7.439 \times 10^{-5}$ at low rotation, while it reaches $2.601 \times 10^{-4}$ at the extreme limit $a_* = 1$. In the right panel, the angular momentum loss rate approaches $8.886 \times 10^{-5}$ at low rotation, while the emission rate is $6.853 \times 10^{-4}$ at $a_* = 1$. These figures are taken from Ref. [14].

When $h = 0$, Eq. (2.40) becomes $\dot{a}_* = 0$. This means that the Kerr black hole continues to lose mass with a nonzero constant value, $a_* = a_{*0}$. Since the mass loss rate is always positive throughout the Hawking process, the function $f$ must be positive definite. If $dh/da_*$ is positive at a point where $h = 0$, the black hole will asymptotically evolve toward a stable state. If $dh/da_*$ is negative or zero at the point, then it represents an unstable equilibrium point of $a_*$, and the black hole will evolve away from it.

### 2.2.3 Results

In Ref. [14], Chambers *et al.* numerically calculated the functions $f(a_*)$ and $g(a_*)$ at 18 values of $a_*$ ranging from $a_* = 1 \times 10^{-4}$ to $a_* = 0.99$. They extrapolate these values to $a_* = 0$ and $a_* = 1$ and interpolate for points of interest.

Fig. 2 shows the behavior of the mass and angular momentum loss rate as a function of the specific angular momentum, described in a scale invariant way by the function $f(a_*)$ and $g(a_*)$, respectively. The loss of mass and angular momentum by emission of scalar particles are more effective at high values of $a_*$. The functions $f(a_*)$ and $g(a_*)$ is used to determine $h(a_*)$ in the following.

Fig. 3 shows the behavior of $h(a_*)$. The most important feature is that $h(a_*) = 0$ at a value of $a_* \simeq 0.555$ as seen in the figure. Because a black hole that forms with a value of $a_* > 0.555$ will have $h(a_*) > 0$, $\dot{a}_*$ will be negative by Eq. (2.40) and the value of $a_*$ will decrease as the black hole evaporates, approaching $a_* = 0.555$. In contrast, because a black hole that forms with $a_* < 0.555$ will have $h(a_*) < 0$, $\dot{a}_*$ will be positive and the value of $a_*$ will increase towards $a_* = 0.555$. Thus, a Kerr black hole emitting massless scalar

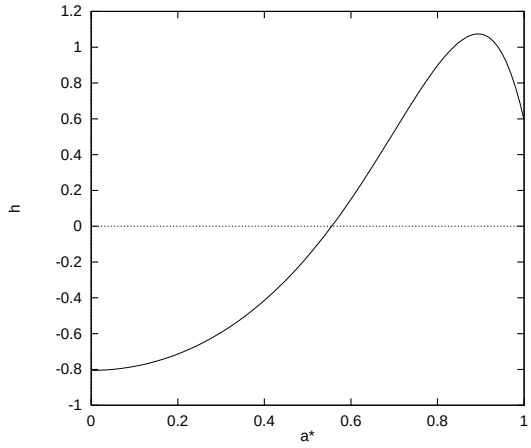


Figure 3: The function $h(a_*)$, Eq. (2.41), is plotted as a function of $a_*$. The point at which $h(a_*) = 0$ occurs at $a_* = 0.555$. A hole formed with $a_*$ on either side of this value will evolve to a state characterized by this value. This figure is taken from Ref. [14].

particles will evolve towards a state with $a_* \simeq 0.555$.

## 2.3 Evolution of a evaporating Myers-Perry black hole

In this subsection, we discuss the evolution of a five-dimensional rotating black hole emitting scalar particles via the Hawking process for arbitrary initial values of the two rotation parameters $a$ and $b$. It is found that any such black hole whose initial rotation parameters both nonzero evolves toward an asymptotic stat $a/M_{MP}^{1/2} = b/M_{MP}^{1/2}$ =const.($\neq 0$), where this constant is independent of the initial values of $a$ and $b$.

### 2.3.1 Myers-Perry solution

The metric of a 5-dimensional rotating black hole is given in the Boyer-Lindquist coordinates as

$$\begin{aligned} ds^2 =& -dt^2 + (r^2 + a_1^2)(d\mu_1^2 + \mu_1^2 d\phi_1^2) + (r^2 + a_2^2)(d\mu_2^2 + \mu_2^2 d\phi_2^2) \\ &+ \frac{\Pi\mathcal{F}}{\Pi - \mu r^2} dr^2 + \frac{\mu r^2}{\Pi\mathcal{F}} (dt + a_1\mu_1^2 d\phi_1 + a_2\mu_2^2 d\phi_2)^2, \end{aligned} \tag{2.42}$$

where

$$\mathcal{F} = 1 - \frac{a_1^2\mu_1^2}{r^2 + a_1^2} - \frac{a_2^2\mu_2^2}{r^2 + a_2^2}, \qquad \Pi = (r^2 + a_1^2)(r^2 + a_2^2). \tag{2.43}$$

The metric (2.42) has three parameters. $\mu$ gives the black hole mass $M_{MP}$ as

$$M_{MP} = \frac{3\pi}{8G}\mu, \tag{2.44}$$

where $G$ is the five-dimensional gravitational constant. For later convenience, using this parameter, we define a typical scale length as $r_s := \sqrt{\mu}$. The rotation parameters $a_1$ and $a_2$ give the angular momenta $J_\phi$ and $J_\psi$ as

$$J_\phi^{(MP)} = \frac{2M_{MP}}{3}a_1, \qquad J_\psi^{(MP)} = \frac{2M_{MP}}{3}a_2. \tag{2.45}$$

The variables $\mu_1$ and $\mu_2$ obey a constraint

$$\mu_1^2 + \mu_2^2 = 1. \tag{2.46}$$

Instead of keeping the symmetric form of the metric (2.42), we solve the constraint (2.46) explicitly. We use the following parametrization

$$\mu_1 = \sin\theta, \qquad \mu_2 = \cos\theta, \tag{2.47}$$

and introduce the following notations

$$a = a_1, \qquad b = a_2, \qquad \phi = \phi_1, \qquad \psi = \phi_2, \tag{2.48}$$

$$\rho^2 = r^2 + a^2\cos^2\theta + b^2\sin^2\theta, \tag{2.49}$$

$$\Delta = (r^2 + a^2)(r^2 + b^2) - \mu r^2. \tag{2.50}$$

Then the metric (2.42) takes the form

$$\begin{aligned} ds^2 =& -dt^2 + (r^2 + a^2)\sin^2\theta d\phi^2 + (r^2 + b^2)\cos^2\theta d\psi^2 \\ &+ \frac{\mu}{\rho^2}\left[dt + a\sin^2\theta d\phi + b\cos^2\theta d\psi\right]^2 + \frac{r^2\rho^2}{\Delta}dr^2 + \rho^2 d\theta^2. \end{aligned} \tag{2.51}$$

Three angles take the following values:

$$0 < \phi, \psi < 2\pi, \qquad 0 < \theta < \pi/2. \tag{2.52}$$

The metric (2.51) is invariant under the following transformation

$$a \leftrightarrow b, \qquad \theta \leftrightarrow \frac{\pi}{2} - \theta, \qquad \phi \leftrightarrow \psi. \tag{2.53}$$

It possesses 3 Killing vectors, $\partial_t$, $\partial_\phi$ and $\partial_\psi$. The event horizon and the inner horizon of the black hole are located at $r_+$ and $r_-$ respectively, where

$$r_\pm^2 = \frac{1}{2}\left[\mu - a^2 - b^2 \pm \sqrt{(\mu - a^2 - b^2)^2 - 4a^2b^2}\right]. \tag{2.54}$$

The angular velocities $\Omega_a$ and $\Omega_b$ are

$$\Omega_a = \frac{a}{r_+^2 + a^2}, \qquad \Omega_b = \frac{b}{r_+^2 + b^2}. \tag{2.55}$$

The temperature and surface gravity of the horizon are

$$T_{MP} = \frac{\kappa_{MP}}{2\pi}, \qquad \kappa_{MP} = \frac{r_+^2 - r_-^2}{2M_{MP}r_+}. \tag{2.56}$$

From the condition for the existence of horizon(s), we obtain the condition $a + b \leq r_s$ constraining the angular momenta. In terms of the nondimensional rotation parameter $a_* := a/r_s$ and $b_* := b/r_s$, the condition becomes

$$a_* + b_* \leq 1. \tag{2.57}$$

Note that we can assume that $a \leq 0$ and $b \leq 0$ without loss of generality.

### 2.3.2 Formulation

First, we formulate the time evolution of the Myers-Perry black hole. To quantize a massless scalar field $\Phi$, we expand it as $\Phi = R(r)\Theta(\theta)e^{im\phi}e^{in\psi}e^{-i\omega t}$. Nomura *et al.* evaluated the emission rates of the total energy and angular momenta by calculating the vacuum expectation value of the energy-momentum tensor of the scalar field (Note that this method to determine the emission rates is different from the method used in Sec. 2.2). Then, the emission rates of the black hole mass $M_{MP}$ and angular momenta $J_\phi$ and $J_\psi$ are given by [1]

$$-\frac{d}{dt}\begin{pmatrix} M_{MP} \\ J_\phi^{(MP)} \\ J_\psi^{(MP)} \end{pmatrix} = \frac{1}{2\pi}\sum_{lmn}\int_0^\infty d\omega \frac{\Gamma_{lmn}^{(MP)}(\omega)}{e^{\omega_+/T_{MP}}-1}\begin{pmatrix} \omega \\ m \\ n \end{pmatrix}. \tag{2.58}$$

Here, $\omega_+ = \omega - m\Omega_\phi - n\Omega_\psi$, $l$ is the eigenvalue of the angular function $\Theta(\theta)$ and $\Gamma_{lmn}^{(MP)}(\omega)$ is the greybody factor.

Similarly to Sec. 2.2, we introduce scale invariant rates of change for the mass and angular momenta of an evaporating black hole as

$$f := -r_s^2\dot{M}_{MP} \qquad g_a := -\frac{r_s}{a_*}\dot{J}_\phi^{(MP)}, \qquad g_b := -\frac{r_s}{b_*}\dot{J}_\psi^{(MP)}, \tag{2.59}$$

where the dot ( $\dot{}$ ) denotes the derivative with respect to $t$. In terms of the scale invariant functions $f$, $g_a$ and $g_b$, the time evolution equations for $a_*$ and $b_*$ are given by

$$\frac{\dot{a}_*}{a_*} = -\frac{8}{3\pi}\frac{fh_a}{r_s^4}, \qquad \frac{\dot{b}_*}{b_*} = -\frac{8}{3\pi}\frac{fh_b}{r_s^4}, \tag{2.60}$$

where the dimensionless functions $h_a$ and $h_b$ are defined as

$$h_a := \frac{3}{2}\left(\frac{g_a}{f} - 1\right), \qquad h_b := \frac{3}{2}\left(\frac{g_b}{f} - 1\right). \tag{2.61}$$

The evolution of $a_*$ and $b_*$ are determined through numerical evaluation of $f$, $g_a$ and $g_b$. In the evolution of Eq. (2.60), a fixed point $h_a = 0$ and $h_b = 0$ plays an important role. Because the mass of an evaporating black hole decreases throughout the Hawking process, $f$ is positive definite. If $h_a > 0$, then $a_*$ decreases, while if $h_a < 0$, then $a_*$ increases. Because $h_a$ depends not only on $a_*$ but also on $b_*$, $h_a = 0$ gives a curve in the $a_*$-$b_*$ plane.

[1] The formulas expressed here have different forms from the original ones in Ref. [16] because of the different definitions of the greybody factor.

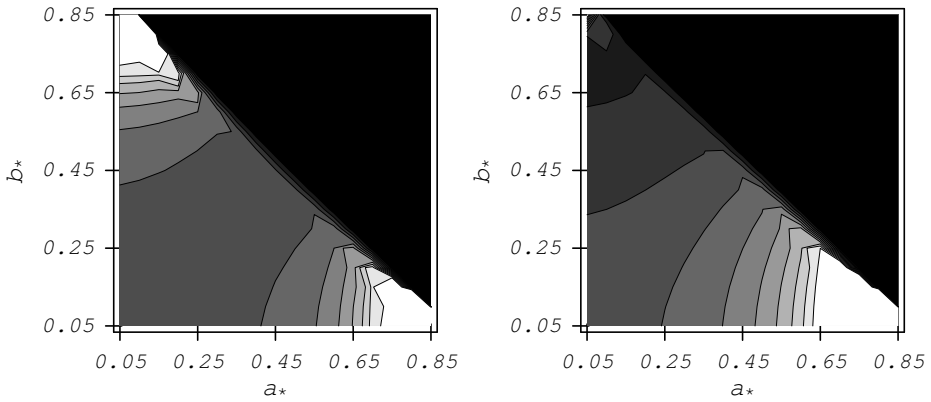


Figure 4: The contours of $f$(left panel) and $g_a$(right panel) in the $a_*$-$b_*$ plane. The black regions correspond to zero, which is forbidden because there is no horizon in this region.. The white regions correspond to the maximums, $f_{\max} \simeq f(0.85, 0.05) = 4.349$ and $g_{a,\max} \simeq f(0.85, 0.05) = 5.92467$. The difference between two contours is $f_{\max}/10$ in the left panel and $g_{a,\max}/10$ in the right panel. These figures are taken from Ref. [16].

### 2.3.3 Results

In order to investigate the time evolution of $a_*$ and $b_*$, we have to analyze Eq. (2.60). In the following analysis, we use units such that $r_s = 1$. For this purpose, the contour plots of $f$ and $g_a$ are depicted in Fig. 4 ($g_b$ is obtained by exchanging the axes for $a_*$ and $b_*$). In the $a_*$-$b_*$ plane, the regions in which $a_* + b_* > 1$ is forbidden because there is no horizon (the black regions in Fig. 4). Two white regions in the left panel show that $f$ becomes large, i.e., the emission rate is high. In the right panel, there is only one white region where the angular momentum $J_\phi$ is emitted effectively. If the two rotation parameters are equal (i.e. $a_* = b_*$), the emission rates are suppressed even if the black hole is in a maximally rotating state ($a_* = b_* = 0.5$). In fact, the angular equation for $\Theta(\theta)$ in this case is exactly the same as that for the Schwarzschild black hole [23]. This is consistent with the result given in Ref. [24].

Fig. 5 shows the evolution of a black hole in the $a_*$-$b_*$ plane. The vector field $(\dot{a}_*, \dot{b}_*)$ with arrows means how the values of $a_*$ and $b_*$ evolve toward the fixed point. The arrows far from the symmetry line of $a_* = b_*$ are very large. Then, if the initial value of $a_*$ (or $b_*$) is large, $a_*$ and $b_*$ approach the same value fast. Near the fixed point $(a_*, b_*) = (a_*^{(\mathrm{cr})}, a_*^{(\mathrm{cr})}) \approx (0.1975, 0.1975)$, the arrows are very small, which means that the evolution toward the fixed point is slow. We thus find that after reaching a state with $a_* = b_*$, $a_*$ and $b_*$ eventually evolve together toward the fixed point $(a_*^{(\mathrm{cr})}, a_*^{(\mathrm{cr})})$. This means that any rotating black hole with two nonzero rotation parameters will evolve toward a final state with the same specific angular momenta, $a_* = b_* = a_*^{(\mathrm{cr})}$. On the

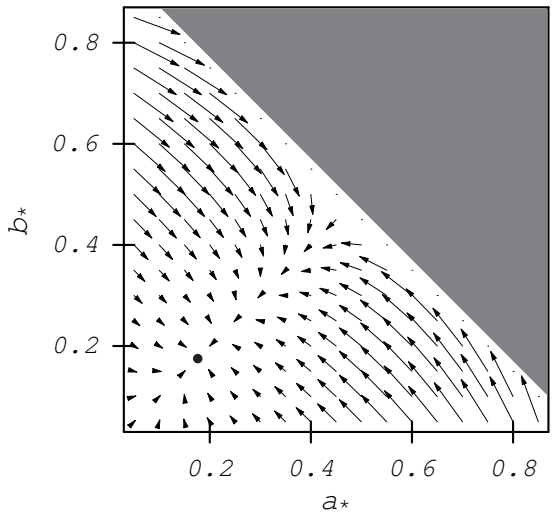


Figure 5: The vector field describes the direction in which $a_*$ and $b_*$ evolve, i.e. $(\dot{a}_*, \dot{b}_*)$. For any initial values of $a_*$ and $b_*$, the system evolves toward $a_* = b_* = 0.1975$ (the black spot), which is a stable fixed point. The shaded region is forbidden. This figure is taken from Ref. [16].

other hand, for a black hole with only one nonzero rotation parameter, i.e. $a \neq 0$ but $b = 0$ exactly, the stable fixed point is $a_* \approx 0.1183$, which is determined by the equation $h_a(a_*, 0) = 0$.

In the above analysis, the dynamical system of Eq. (2.60) has one stable attractor, which can be reached through the Hawking evaporation. However, the black hole may evaporate away before this fixed point is reached. This happens if the evaporation time, $\tau_M = -M/\dot{M}$, is longer than the evolution time scale in the $a_*$-$b_*$ plane, $\tau_{a_*} = a_*/|\dot{a}_*|$. Therefore, if the initial mass of the black hole is sufficiently large, the two specific angular momenta will become equal in the Hawking process.

# 3 Black rings

In this section, we review basic properties of black rings. In addition, we show that for a doubly spinning black ring, there is a limit in which the ring very thin and locally it approaches the geometry of a boosted Kerr black string. This limit was discussed in the more general case of an unbalanced Pomeransky-Sen'kov black ring in Ref. [25].

## 3.1 An Emparan-Reall black ring

In this subsection, we review a singly spinning black ring.

### 3.1.1 Emparan-Reall solution

The black ring metic is given by

$$\begin{aligned} ds^2 =& -\frac{F(x)}{F(y)}\left(dt + R\sqrt{\lambda\nu}(1+y)d\psi\right)^2 \\ &+\frac{R^2}{(x-y)^2}\Bigg[-F(x)\left(G(y)d\psi^2 + \frac{F(y)}{G(y)}dy^2\right) \\ &\qquad + F(y)^2\left(\frac{dx^2}{G(x)} + \frac{G(x)}{F(x)}d\phi^2\right)\Bigg], \end{aligned} \tag{3.1}$$

with

$$F(\xi) = 1-\lambda\xi, \qquad G(\xi) = (1-\xi^2)(1-\nu\xi). \tag{3.2}$$

Note that the form of the solution is not a original one obtained in Ref. [4], but the one revised in Ref. [26]. This solution is characterized by the following three parameters: a length scale R and dimensionless parameters $\lambda$ and $\nu$.

The range of $\nu$ and $\lambda$ are

$$0 \le \nu < \lambda < 1. \tag{3.3}$$

In order to avoid a closed timelike curve, we restrict the $x$ range to

$$-1 \le x \le 1. \tag{3.4}$$

The $y$ range is

$$-\infty < y \le -1, \qquad \lambda^{-1} < y < \infty. \tag{3.5}$$

$|y| = \infty$ is a ergoshere, $y = 1/\nu$ is a event horizon, $y = 1/\lambda$ is a singularity inside the event horizon.

In this metric, the surface "$t, y, \psi =$ const." corresponds to $S^2$ and $x$ and $\phi$ are their coordinates. On the other hand, the curve "$t, y, x, \phi =$const." corresponds to $S^1$ and $\psi$ is its coordinate. Therefore, the whole represents a ring-shape $S^1 \times S^2$.

$\nu$ parametrize the radius of $S^2$. We recover a very thin black ring as $\nu \to 0$. At the opposite limit, the solution represents a very fat black ring as $\nu \to 1$.

### 3.1.2 Conical singularities

The solution generally has conical singularities. We eliminate them because we will consider the balanced black ring(, i.e. the black ring with no conical singularities,) below. Considering an small circle around an axis, we impose the condition for a length of an arc $\ell$ and an radius $r$.

$$2\pi = \ell/r \tag{3.6}$$

First, we obtain the period $\Delta\phi$ of $\phi$ at $x=-1$. Using

$$\ell = \int_0^{\Delta\phi} \sqrt{g_{\phi\phi}} d\phi = \Delta\phi \frac{RF(y)}{(x-y)} \sqrt{\frac{G(x)}{F(x)}}, \tag{3.7}$$

$$r = \int_{-1}^{x} \sqrt{g_{xx}} dx = \int_{-1}^{x} \frac{RF(y)}{(x-y)} \frac{dx}{\sqrt{G(x)}}, \tag{3.8}$$

the condition for avoiding the conical singularity is

$$\begin{aligned} 2\pi &= \lim_{x\to -1} \frac{\ell}{r} \\ &= \frac{\left(\lim \Delta\phi \frac{RF(y)}{(x-y)}\right)\left(\lim \sqrt{\frac{G(x)}{F(x)}}\right)}{\lim \int_{-1}^{x} \frac{RF(y)}{(x-y)} \frac{dx}{\sqrt{G(x)}}} \\ &= \frac{\left(\Delta\phi \frac{RF(y)}{(-1-y)}\right)\left(\frac{1}{2}\sqrt{\frac{G(-1)}{F(-1)}} \frac{G'(-1)F(-1)-G(-1)F'(-1)}{F^2(-1)}\right)}{\frac{RF(y)}{(-1-y)} \frac{1}{\sqrt{G(-1)}}} \\ &= \Delta\phi \frac{G'(-1)}{2\sqrt{F(-1)}}. \end{aligned} \tag{3.9}$$

Here we use

$$\lim_{x\to x_0} \frac{G(x)}{F(x)} = \lim_{x\to x_0} \frac{G'(x)}{F'(x)}. \tag{3.10}$$

Therefore, the period of $\phi$ is

$$\Delta\phi = \frac{4\pi\sqrt{F(-1)}}{G'(-1)} = \frac{2\pi\sqrt{1+\lambda}}{1+\nu}. \tag{3.11}$$

As a similar way, one can obtain the period $\Delta\psi$ of $\psi$ at $y=-1$ is

$$\Delta\psi = \Delta\phi. \tag{3.12}$$

The period $\Delta\phi'$ of $\phi$ at $x=+1$ is

$$\Delta\phi' = \frac{4\pi\sqrt{F(+1)}}{|G'(+1)|} = \frac{2\pi\sqrt{1-\lambda}}{1-\nu}. \tag{3.13}$$

In addition, $\Delta\phi'$ and $\Delta\phi$ should be identical to each other because they are the periods of the same $\phi$:

$$\Delta\phi' = \Delta\phi. \tag{3.14}$$

Using $\lambda$ and $\nu$, we rewrite this condition.

$$\lambda = \frac{2\nu}{1+\nu^2}. \tag{3.15}$$

### 3.1.3 Asymptotical flatness

We check asymptotical flatness of the black ring metric at $x = y = -1$. First, we make the periods of $\psi$ and $\phi$ $2\pi$ with

$$\tilde{\psi} = \frac{2\pi}{\Delta\psi}\psi, \qquad \tilde{\phi} = \frac{2\pi}{\Delta\phi}\phi \tag{3.16}$$

In addition, we define new coordinates $\zeta$ and $\eta$ as

$$\zeta = \frac{\tilde{R}\sqrt{-1-y}}{(x-y)}, \qquad \eta = \frac{\tilde{R}\sqrt{x+1}}{(x-y)} \tag{3.17}$$

with

$$\tilde{R} = \frac{\sqrt{2}(1+\lambda)}{\sqrt{1+\nu}}R. \tag{3.18}$$

Therefore, the metric at $x = y = -1$

$$ds^2 \sim -dt^2 + d\zeta^2 + \zeta^2 d\tilde{\psi}^2 + d\eta^2 + \eta^2 d\tilde{\phi}^2. \tag{3.19}$$

It can be found that the black ring solution is asymptotically flat.

### 3.1.4 Physical quantities

Using the three parameters $\nu$, $\lambda$, $R$, we show the physical quantities for the Emparan-Reall black ring. Note that "$\to$" means that we impose the balance condition (3.15).

The mass and angular momentum along $S^1$ are

$$M = \frac{3\pi R^2}{4G}\frac{\lambda(\lambda+1)}{1+\nu} \to \frac{3\pi R^2}{4G}\frac{2\nu(1+\nu)}{(1+\nu^2)^2}, \tag{3.20}$$

$$J_\psi = \frac{\pi R^3}{2G}\frac{\sqrt{\lambda\nu}(1+\lambda)^{5/2}}{(1+\nu)^2} \to \frac{\pi R^3}{2G}\sqrt{\frac{2\nu^2(1+\nu)^3}{(1-\nu)^3(1+\nu^2)^3}}. \tag{3.21}$$

Of course, the angular momentum along $S^2$ is $J_\phi \equiv 0$. The area and temperature of the horizon are

$$A_H = 8\pi^2 R^3 \frac{\lambda^{1/2}(1+\lambda)(\lambda-\nu)^{3/2}}{(1+\nu)^2(1-\nu)} \to 8\pi^2 R^3 \frac{\nu^2\sqrt{2(1-\nu)(1+\nu)^3}}{(1+\nu^2)^3}, \tag{3.22}$$

$$T_H = \frac{\kappa}{2\pi} = \frac{1}{4\pi R}\frac{1-\nu}{\sqrt{\lambda(\lambda-\nu)}} \to \frac{1}{4\pi R}\frac{1+\nu^2}{\sqrt{2}}\sqrt{\frac{1-\nu}{1+\nu}}, \tag{3.23}$$

where $\kappa$ is the surface gravity of the horizon.

### 3.1.5 Non-uniqueness

We focus on the angular momentum normalized by mass

$$j^2 := \frac{27\pi}{32G}\frac{J^2}{M^3} = \frac{(1+\nu)^3}{8\nu}. \tag{3.24}$$

One easily sees that it is infinite at $\nu = 0$, decrease to a minimum value $27/32$ at $\nu = 1/2$, and then grows to 1 at $\nu = 1$. This implies that in the range

$$\frac{27}{32} \leq j^2 < 1 \tag{3.25}$$

there exist two black rings with the same value of the spin for fixed mass. This regime of non-uniqueness occurs when the parameter $\nu$ takes values in

$$\sqrt{5} - 2 \leq \nu < 1. \tag{3.26}$$

### 3.1.6 Thin ring limit

There is a limit in which the ring very thin and locally it approaches the geometry of a boosted black string. To recover this limit, we focus on a region near the horizon

$$R \to \infty, \qquad \lambda \to 0, \qquad \nu \to 0 \tag{3.27}$$

while keeping $R\lambda$ and $R\nu$ the following finite value:

$$R\lambda = r_H \cosh\sigma, \qquad R\nu = r_H \sinh\sigma. \tag{3.28}$$

Here, we introduced new parameters $r_H$ and $\sigma$. We also define new coordinates $r, \theta$, and $z$ as

$$r = -R\frac{F(y)}{y}, \qquad \cos\theta = x, \qquad z = R\psi. \tag{3.29}$$

The black ring metric (3.1) matches a boosted Schwarzschild black string

$$ds^2 = -\bar{f}\left(dt - \frac{r_H \sinh 2\sigma}{2r\bar{f}}dz\right)^2 + \frac{f}{\bar{f}}dz^2 + \frac{1}{f}dr^2 + r^2 d\Omega \tag{3.30}$$

with

$$f = 1 - \frac{r_H}{r}, \qquad \bar{f} = 1 - \frac{r_H \cosh^2\sigma}{r}. \tag{3.31}$$

We can find from the metric that $r_H$ is a Schwarzschild radius and $\sigma$ is a boost parameter. Due to the balance condition, the boost parameter takes the constant value, $\sigma = \arctan(1/\sqrt{2})$.

## 3.2 A Pomeransky-Sen'kov black ring

In this subsection, we review a doubly spinning black ring. This is the extension of the Emparan-Reall black ring.

### 3.2.1 Pomeransky-Sen'kov solution

The metric of the Pomeransky-Sen'kov black ring is [10]

$$\begin{aligned} ds^2 =& -\frac{H(y,x)}{H(x,y)}\left(dt+\Omega\right)^2 - \frac{F(x,y)}{H(y,x)}d\psi^2 - 2\frac{J(x,y)}{H(y,x)}d\psi d\phi \\ &+ \frac{F(y,x)}{H(y,x)}d\phi^2 + \frac{2R^2H(x,y)}{\left(x-y\right)^2\left(1-\nu\right)^2}\left(\frac{dx^2}{G(x)} - \frac{dy^2}{G(y)}\right), \end{aligned} \tag{3.32}$$

where the 1-form $\Omega$ is

$$\begin{aligned} \Omega =& -\frac{2R\lambda\sqrt{\left(1+\nu\right)^2-\lambda^2}}{H(y,x)}\Big[\left(1-x^2\right)y\sqrt{\nu}d\phi \\ &+ \frac{1+y}{1-\lambda+\nu}\left\{1+\lambda-\nu+x^2y\nu\left(1-\lambda-\nu\right)+2\nu x\left(1-y\right)\right\}d\psi\Big], \end{aligned} \tag{3.33}$$

and the functions $G, H, J$ and $F$ are

$$G(x) = \left(1-x^2\right)\left(1+\lambda x+\nu x^2\right), \tag{3.34}$$

$$\begin{aligned} H(x,y) =& 1+\lambda^2-\nu^2+2\lambda\nu\left(1-x^2\right)y \\ &+ 2x\lambda\left(1-y^2\nu^2\right)+x^2y^2\nu\left(1-\lambda^2-\nu^2\right), \end{aligned} \tag{3.35}$$

$$\begin{aligned} J(x,y) =& \frac{2R^2\left(1-x^2\right)\left(1-y^2\right)\lambda\sqrt{\nu}}{\left(x-y\right)\left(1-\nu\right)^2} \\ &\times\left[1+\lambda^2-\nu^2+2\left(x+y\right)\lambda\nu-xy\nu\left(1-\lambda^2-\nu^2\right)\right], \end{aligned} \tag{3.36}$$

$$\begin{aligned} F(x,y) =& \frac{2R^2}{\left(x-y\right)\left(1-\nu\right)^2} \\ &\times\Big[G(x)\left(1-y^2\right)\left[\left\{\left(1-\nu\right)^2-\lambda^2\right\}\left(1+\nu\right)+y\lambda\left(1-\lambda^2+2\nu-3\nu^2\right)\right] \\ &+G(y)\big[2\lambda^2+x\lambda\left\{\left(1-\nu\right)^2+\lambda^2\right\}+x^2\left\{\left(1-\nu\right)^2-\lambda^2\right\}\left(1+\nu\right) \\ &+x^3\lambda\left(1-\lambda^2-3\nu^2+2\nu^3\right)-x^4(1-\nu)\nu\left(-1+\lambda^2+\nu^2\right)\big]\Big]. \end{aligned} \tag{3.37}$$

Here, we follow the notation of Ref. [10] except that we choose the signature $(-,+,+,+,+)$ for the metric, exchange $\phi$ and $\psi$, and use $R$ instead of $k$. The coordinate ranges are $-\infty < t < +\infty$, $0 < \phi, \psi < 2\pi$, $-1 \leq x \leq 1$ and $-\infty < y < -1$. $R$ is a parameter of dimension of length, which determines the characteristic scale of the $S^1$ radius. $\lambda$ and $\nu$ are dimensionless parameters satisfying $0 \leq \nu < 1$ and $2\sqrt{\nu} \leq \lambda < 1+\nu$, which determine two nondimensional rotation parameters. The regular event horizon exists at $y = y_h$, where

$$y_h = \frac{-\lambda+\sqrt{\lambda^2-4\nu}}{2\nu}. \tag{3.38}$$

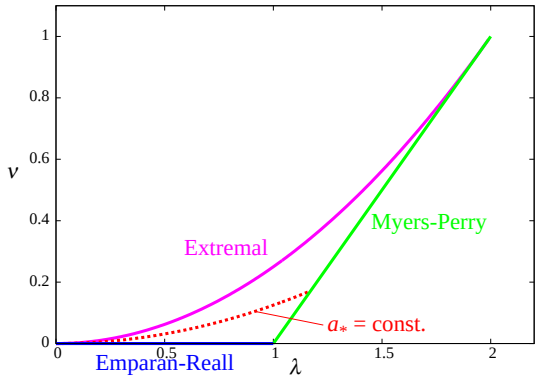


Figure 6: The parameter space $(\lambda, \nu)$ of the Pomeransky-Sen'kov solution. $\lambda$ and $\nu$ can take values in the region surrounded by solid lines. The line $\nu = \lambda - 1$ is the Myers-Perry black hole limit, the line $\nu = 0$ is the Emparan-Reall black ring limit, and the line $\nu = \lambda^2/4$ is the extremal limit. The point $\lambda = \nu = 0$ corresponds to the boosted Kerr string limit. The broken line $\nu = a_*^2\lambda^2/4$ is the path to the point $\lambda = \nu = 0$ with a fixed $a_*$.

The solution is asymptotically flat and the spacelike infinity is located at $x = y = -1$. This becomes clear when the new coordinates $(r_1, r_2)$ are introduced by the set of equations:

$$r_1 r_2 = -\frac{4k^2 G(x)G(y)}{(x-y)^2(1-\nu)}, \qquad \frac{r_1^2 - 2_2^2}{2} = \frac{k^2(1-xy)\left[2 + (x+y)\lambda + 2xy\nu\right]}{(x-y)^2(1-\nu)} \tag{3.39}$$

In the new coordinates the flat space metric at $x = y = -1$ has the form:

$$d\ell^2 = dr_1^2 + dr_2^2 + r_1^2 d\psi^2 + r_2^2 \phi^2. \tag{3.40}$$

The coordinates $(x, \phi)$ parametrize the two-sphere $S^2$ and $\psi$ parametrizes the circle $S^1$. One recovers the Emparan-Reall black ring by setting $\nu = 0$, and the line $\nu = \lambda^2/4$ represents the sequence of extremal black rings (see Fig. 6).

### 3.2.2 Physical quantities

The mass and angular momenta are

$$M = \frac{3\pi R^2 \lambda}{G(1-\lambda+\nu)}, \qquad J_\phi = \frac{4\pi R^3 \lambda\sqrt{\nu}\sqrt{(1+\nu)^2 - \lambda^2}}{G(1-\nu)^2(1-\lambda+\nu)}, \tag{3.41}$$

$$J_\psi = \frac{2\pi R^3 \lambda(1+\lambda-6\nu+\lambda\nu+\nu^2)\sqrt{(1+\nu)^2-\lambda^2}}{G(1-\nu)^2(1-\lambda+\nu)^2}. \tag{3.42}$$

The angular velocities, the area, and the surface gravity of the horizon are written as [7]

$$\Omega_\phi = \frac{\lambda(1+\nu)-(1-\nu)\sqrt{\lambda^2-4\nu}}{4R\lambda\sqrt{\nu}}\sqrt{\frac{1+\nu-\lambda}{1+\nu+\lambda}}, \qquad \Omega_\psi = \frac{1}{2R}\sqrt{\frac{1+\nu-\lambda}{1+\nu+\lambda}}, \tag{3.43}$$

$$A_H = \frac{32\pi^2 R^3\lambda(1+\nu+\lambda)}{(1-\nu)^2(y_h^{-1}-y_h)}, \qquad \kappa = \frac{(y_h^{-1}-y_h)(1-\nu)\sqrt{\lambda^2-4\nu}}{4R\lambda(1+\nu+\lambda)}. \tag{3.44}$$

The Pomeransky-Sen'kov solution has no conical singularities. The general doubly spinning black ring with conical singularities and the way to eliminate them are discussed in Ref. [27].

The angular momenta normalized by mass are

$$j_\psi := \frac{27\pi}{32G}\frac{J_\psi^2}{M^3} \geq \frac{3}{4}, \qquad j_\phi \equiv \frac{27\pi}{32G}\frac{J_\phi^2}{M^3} \leq \frac{1}{4}. \tag{3.45}$$

There is the lower limit on the angular momentum along $\psi$. On the other hand, there is the upper limit on the angular momentum along $\phi$.

### 3.2.3 Thin ring limit

We consider a thin ring limit $\lambda \to 0$ where the ratio of the $S^2$ radius to the $S^1$ radius becomes very small. Here, we have to take care of the fact that this limit depends on the path to the point $\lambda = \nu = 0$. For example, taking the limit $\lambda \to 0$ on the line $\nu = 0$ gives the boosted Schwarzschild string, while taking the limit $\lambda \to 0$ on the extremal line $\nu = \lambda^2/4$ should result in the extremal Kerr black string. Therefore, $\lambda = \nu = 0$ is a degenerate point, and in order to resolve this degeneracy, we introduce a new parameter $a_*$ as

$$\nu = \frac{1}{4}a_*^2\lambda^2, \tag{3.46}$$

and consider a limit $\lambda \to 0$ on the line of a fixed $a_*$ (see Fig. 6). Also, in order to obtain a well-defined limit, we introduce

$$M_K = \frac{1}{\sqrt{2}}\lambda R, \tag{3.47}$$

and fix $M_K$ in taking this limit.

We introduce the new coordinates $r$, $z$ and $\theta$ as

$$y = -\frac{\sqrt{2}R}{r}, \qquad \psi = -\frac{z}{\sqrt{2}R}, \qquad x = \cos\theta, \tag{3.48}$$

and collect the leading-order term of each metric component with respect to $\lambda$. In the limit $\lambda \to 0$, the functions in the metric can be approximated by

$$G(x) \sim \sin^2\theta \tag{3.49}$$

$$G(y) \sim -\frac{R^2}{r^2}\left(1 - \frac{2M_K}{r} + \frac{a^2}{r}\right) \tag{3.50}$$

$$H(x,y) \sim 1 + \frac{a^2\cos^2\theta}{r^2} \tag{3.51}$$

$$H(y,x) \sim 1 - \frac{4M_K}{r} + \frac{a^2\cos^2\theta}{r^2} \tag{3.52}$$

$$J(x,y) \sim -R\frac{2\sqrt{2}M_K a\sin^2\theta}{r} \tag{3.53}$$

$$F(x,y) \sim -2R^2\left[1 - \frac{2M_K}{r} + \frac{a^2\cos^2\theta}{r^2}\right] \tag{3.54}$$

$$\begin{aligned} F(y,x) \sim \frac{\sin^2\theta}{M_K^4 r^2}\Big[&r^4 - 4M_K r^3 + r^2a^2(1+\cos^2\theta) \\ &- 2M_K^2 ra^2(1+\cos^2\theta) + a^4\cos^2\theta\Big] \end{aligned} \tag{3.55}$$

$$\Omega \sim \frac{2\sqrt{2}M_K/r}{H(y,x)}\left(a\sin^2\theta d\phi - dz\right) \tag{3.56}$$

Then, the black ring solution is reduced to the so-called boosted Kerr string solution

$$\begin{aligned} ds^2 = &-\left(1 - \frac{2M_K r\cosh^2\sigma}{\rho^2}\right)dt^2 + \frac{2M_K r\sinh 2\sigma}{\rho^2}dtdz \\ &+ \left(1 + \frac{2M_K r\sinh^2\sigma}{\rho^2}\right)dz^2 + \frac{\rho^2}{\Delta}dr^2 + \rho^2 d\theta^2 \\ &+ \frac{\left(r^2+a^2\right)^2 - \Delta a^2\sin^2\theta}{\rho^2}\sin^2\theta d\phi^2 \\ &- \frac{4M_K r\cosh\sigma}{\rho^2}a\sin^2\theta dt d\phi - \frac{4M_K r\sinh\sigma}{\rho^2}a\sin^2\theta dz d\phi, \end{aligned} \tag{3.57}$$

where $\rho^2 = r^2 + a^2\cos^2\theta$ and $\Delta = r^2 - 2M_K r + a^2$, and $a$ is defined by $a := M_K a_*$. Since $M_K$ and $a$ are the mass and rotational parameter of a four-dimensional Kerr black hole respectively, $a_*$ represents the nondimensional rotation parameter along $S^2$ direction. $\sigma := \mathrm{arctanh}(1/\sqrt{2})$ is the boost parameter. Although the boost parameter can take any value for a general boosted Kerr string, it is restricted to this value for the thin limit of a black ring. The event horizon is located at $r = r_+$ where $r_\pm := M_K \pm \sqrt{M_K^2 - a^2} = M_K(1 \pm \sqrt{1-a_*^2})$.

In studying the evaporation of a black ring, we use this boosted Kerr string solution in the following sense. We consider the situation where $\lambda$ is very small, and do not take the exact limit. Then, in the neighborhood of the black ring, the spacetime metric can be well approximated by the boosted Kerr string solution. For this reason, the value of $R$ is not infinite in our analysis although it is very large compared to $M_K$. The relative error in this approximation is $O(\lambda)$ compared to the leading order in the following analyses.

In this thin-limit approximation, the physical quantities in Eqs. (3.41)–(3.44) are expressed in terms of $R, M_K$ and $a$ (or $a_*$) as

$$M \simeq 3\sqrt{2}\pi R M_K, \qquad J_\psi \simeq 2\sqrt{2}\pi R^2 M_K, \qquad J_\phi \simeq 4\pi a_* R M_K^2. \tag{3.58}$$

$$\Omega_\phi \simeq \frac{a}{2M_K r_+}\frac{1}{\cosh\sigma}, \qquad \Omega_\psi \simeq \frac{1}{2R}, \tag{3.59}$$

$$A_H \simeq 16\pi^2 r_+ M_K R, \qquad \kappa \simeq \frac{r_+ - r_-}{4M_K r_+}\frac{1}{\cosh\sigma}. \tag{3.60}$$

The inverse relations of Eq. (3.58) are

$$R \simeq \frac{3J_\psi}{2M}, \qquad M_K \simeq \frac{\sqrt{2}}{9\pi}\frac{M^2}{J_\psi}, \qquad a_* \simeq \frac{27\pi}{4}\frac{J_\psi J_\phi}{M^3}, \tag{3.61}$$

and $\lambda$ is expressed as

$$\lambda = \frac{\sqrt{2}M_K}{R} \simeq \frac{4}{27\pi}\frac{M^3}{J_\psi^2}. \tag{3.62}$$

Because $\lambda^{-1/2}$ is proportional to the angular momentum $J_\psi$ normalized by mass $M$, it can be interpreted as the nondimensional rotation parameter along $S^1$. At the same time, Eq. (3.62) also means that $\lambda$ gives the order of the ratio of the $S^2$ radius to the $S^1$ radius. Therefore, $\lambda$ is interpreted as an indicator for the "thickness" of the black ring. In this thesis, we call $\lambda$ the thickness parameter.

### 3.2.4 Effect of boost

Note that $\Omega_\phi$ in Eq. (3.59) is equal to the angular velocity defined by the Killing generator $\xi$ of the horizon of the boosted Kerr string[2],

$$\xi = \partial_t + \Omega_\phi \partial_\phi + V\partial_z \tag{3.63}$$

with

$$V = \tanh\sigma, \tag{3.64}$$

and $\kappa$ in Eq. (3.60) is identical to the surface gravity of the horizon calculated with $\xi$. For a later convenience, it is useful to compare $\Omega_\phi$ and $\kappa$ with the angular velocity and the surface gravity of the horizon of the unboosted Kerr string. In the following, a quantity in the unboosted system is indicated by prime ( $'$ ). In the unboosted system, the Killing generator of the horizon is $\xi' = \partial_{t'} + \Omega'_\phi \partial_\phi$, and $\Omega'_\phi$ and $\kappa'$ calculated from $\xi'$ are

$$\Omega'_\phi = \frac{a}{2M_K r_+}, \qquad \kappa' = \frac{r_+ - r_-}{4M_K r_+}. \tag{3.65}$$

There is a deference in the quantities of the boosted and unboosted systems by a factor of $1/\cosh\sigma$. This is understood as the effect of time delay in the Lorentz boost.

[2]Our expression of $\Omega_\phi$ does not agree with that of Ref. [28] because the definition is different.

# 4 Formulation

In this section, we formulate the time evolution of mass and angular momenta of a thin black ring via Hawking radiation, by approximating the evolution of a scalar field in the black ring spacetime by that in a boosted Kerr string spacetime.

## 4.1 Emission rate

The evolution of a scalar field is governed by the Klein-Gordon equation in the black ring spacetime

$$(-g)^{-1/2}\,\partial_\mu\left(\sqrt{-g}g^{\mu\nu}\partial_\nu\Phi\right)=0, \tag{4.1}$$

where $g$ is the determinant of the black ring metric.

To quantize the field, we need to expand it in terms of the eigenmodes for $\Phi$, which can be written in the black ring background as

$$\Phi = e^{-i\omega t}e^{im\phi}e^{in\psi}\Psi(x,y), \tag{4.2}$$

where $\omega$, $m$ and $n$ are the eigenvalues for the Killing vector fields $\partial_t$, $\partial_\psi$ and $\partial_\phi$, respectively. By inserting this expression into Eq. (4.1), we obtain a second-order elliptic equation for $\Psi(x,y)$ in the $(x,y)$ plane. This equation has a discrete series of regular solutions labeled by an integer $\ell$. In the Schwarzschild string limit with $J_\phi=0$, this series of solutions become proportional to the associate Legendre functions $P_\ell^m(x)$. Thus, the mode functions are labeled by the four parameters $(\omega,\ell,m,n)$ in which $\ell$, $m$ and $n$ take integer values.

Following the discussion in chapter 2, the expected number of particles emitted per unit time for each mode from the black ring is given by

$$\langle N_{\rm BR}\rangle = \frac{\Gamma^{\rm (BR)}_{\ell mn}(\omega)}{e^{(\omega-n\Omega_\psi-m\Omega_\phi)/T_{\rm BR}}-1}, \tag{4.3}$$

where $T_{\rm BR}$ is the temperature of the horizon and $\Gamma^{\rm (BR)}_{\ell mn}(\omega)$ is the greybody factor, which is identical to the absorption probability of the incoming wave of the corresponding modes. This determines the emission rates of the total mass $M$ and angular momenta $J_\psi$ and $J_\phi$ as

$$-\frac{d}{dt}\begin{pmatrix} M \\ J_\psi \\ J_\phi \end{pmatrix} = \frac{1}{2\pi}\sum_{\ell,m,n}\int_0^\infty d\omega\langle N_{\rm BR}\rangle\begin{pmatrix} \omega \\ n \\ m \end{pmatrix}, \tag{4.4}$$

where the summation is taken over all modes. Note that in this expression, it is difficult to estimate the greybody factor generally because we cannot separate the coordinates $x$ and $y$, and two-dimensional numerical calculations are required to determine the energy eigenvalues and corresponding eigenmodes.

In order to circumvent this difficulty, we consider the situation where the mode functions can be approximately evaluated: a black string limit discussed

above. For the boosted black string (3.57), we can separate the wave equation, and therefore, we approximate the evolution of a scalar field in a black ring spacetime by that in a boosted Kerr string spacetime. In this situation, the variables can be separated as

$$\Phi = e^{-i\omega t} R(r) e^{-ikz} e^{im\phi} S_\ell^m(\theta), \tag{4.5}$$

where $S_\ell^m(\theta)$ is the spheroidal harmonic function. From the coordinate transformation (3.48), $n$ of a black ring and $k$ of a boosted black string are related by

$$n = 2kR \tanh\sigma. \tag{4.6}$$

The expected number of particles emitted per unit time per mode is given by

$$\langle N_{\rm BBS} \rangle = \frac{\Gamma_{\ell mn}(\omega)}{e^{(\omega - kV - m\Omega_\phi)/T} - 1}, \tag{4.7}$$

where $T = \kappa/2\pi$ is the temperature of the horizon with $\kappa$ in Eq. (3.60), and $V$ is the linear velocity introduced in Eq. (3.64). $\Gamma_{\ell mn}(\omega)$ is the greybody factor of the boosted Kerr string spacetime. We evaluate the emission rates (4.4) by using $\langle N_{\rm BBS} \rangle$ instead of $\langle N_{\rm BR} \rangle$.

## 4.2 Simplification

We normalize all quantities by the mass density $M_K$,

$$\tilde{\omega} = M_K \omega, \qquad \tilde{k} = M_K k, \qquad \tilde{\Omega}_\phi = M_K \Omega_\phi, \qquad \tilde{T} = M_K T = \frac{M_K \kappa}{2\pi}. \tag{4.8}$$

We change the order of summations over $\ell$ and $m$ as

$$\sum_{\ell=0}^{\infty} \sum_{m=-\ell}^{\ell} = \sum_{m=-\infty}^{\infty} \sum_{\ell=|m|}^{\infty}, \tag{4.9}$$

and introduce

$$g^{(m)}(\tilde{\omega}, \tilde{k}) := \sum_{\ell=|m|}^{\infty} \Gamma_{\ell mn}(\tilde{\omega}), \tag{4.10}$$

where $\tilde{k}$ and $n$ are related to each other by Eq. (4.6). Then, the emission rates can be written as

$$-\frac{d}{dt} \begin{pmatrix} M \\ J_\psi \\ J_\phi \end{pmatrix} = \frac{1}{2\pi M_K} \sum_{m=-\infty}^{\infty} \sum_{n=-\infty}^{\infty} \int_{|\tilde{k}|}^{\infty} d\tilde{\omega} \frac{g^{(m)}(\tilde{\omega}, \tilde{k})}{e^{(\tilde{\omega} - \tilde{k}V - m\tilde{\Omega}_\phi)/\tilde{T}} - 1} \begin{pmatrix} \tilde{\omega}/M_K \\ n \\ m \end{pmatrix}. \tag{4.11}$$

Here, the lower limit of the integral is $|\tilde{k}|$ because the modes with their energy $\omega < |\tilde{k}|$ are gravitationally bounded and do not escape to infinity. Because

the spectral density of $\tilde{k}$ is very large, $O(1/\lambda)$, the summation over $n$ can be replaced by the integral:

$$\sum_n \to \int dn = \frac{2R\tanh\sigma}{M_K}\int d\tilde{k}. \tag{4.12}$$

The relative error produced by this replacement is $O(\lambda)$ and negligible in our thin-limit approximation. We obtain

$$-\frac{dM}{dt} = \frac{R}{\sqrt{2}\pi M_K^3}\sum_{m=-\infty}^{\infty}\int_{-\infty}^{\infty}d\tilde{k}\int_{|\tilde{k}|}^{\infty}d\tilde{\omega}\frac{\tilde{\omega}g^{(m)}(\tilde{\omega},\tilde{k})}{e^{(\tilde{\omega}-\tilde{k}V-m\tilde{\Omega}_\phi)/\tilde{T}}-1}, \tag{4.13}$$

$$-\frac{dJ_\psi}{dt} = \frac{R^2}{\pi M_K^3}\sum_{m=-\infty}^{\infty}\int_{-\infty}^{\infty}d\tilde{k}\int_{|\tilde{k}|}^{\infty}d\tilde{\omega}\frac{\tilde{k}g^{(m)}(\tilde{\omega},\tilde{k})}{e^{(\tilde{\omega}-\tilde{k}V-m\tilde{\Omega}_\phi)/\tilde{T}}-1}. \tag{4.14}$$

$$-\frac{dJ_\phi}{dt} = \frac{R}{\sqrt{2}\pi M_K^2}\sum_{m=-\infty}^{\infty}\int_{-\infty}^{\infty}d\tilde{k}\int_{|\tilde{k}|}^{\infty}d\tilde{\omega}\frac{mg^{(m)}(\tilde{\omega},\tilde{k})}{e^{(\tilde{\omega}-\tilde{k}V-m\tilde{\Omega}_\phi)/\tilde{T}}-1}. \tag{4.15}$$

The integral in each formula can be further simplified if we perform the transformation from $(\tilde{\omega},\tilde{k})$ to $(\tilde{\omega}',\tilde{k}')$,

$$\tilde{\omega} = \tilde{\omega}'\cosh\sigma + \tilde{k}'\sinh\sigma, \qquad \tilde{k} = \tilde{\omega}'\sinh\sigma + \tilde{k}'\cosh\sigma. \tag{4.16}$$

Substituting these formulas with $\cosh\sigma = \sqrt{2}$ and $\sinh\sigma = 1$ and rewriting $M_K$ and $R$ by $M$, $J_\psi$ and $J_\phi$ using Eq. (3.61), we obtain the simplified expression of the evolution:

$$-\frac{1}{M}\frac{dM}{dt} = 2F(a_*)\frac{J_\psi^4}{M^8}, \tag{4.17}$$

$$-\frac{1}{J_\psi}\frac{dJ_\psi}{dt} = 3F(a_*)\frac{J_\psi^4}{M^8}, \tag{4.18}$$

$$-\frac{1}{J_\phi}\frac{dJ_\phi}{dt} = G(a_*)\frac{J_\psi^3}{J_\phi M^5}, \tag{4.19}$$

with

$$F(a_*) := \frac{3^7\pi^2}{2^3\sqrt{2}}\sum_{m=-\infty}^{\infty} I_1^{(m)}(a_*), \tag{4.20}$$

$$G(a_*) := \frac{3^5\pi}{2^2\sqrt{2}}\sum_{m=-\infty}^{\infty} I_2^{(m)}(a_*). \tag{4.21}$$

Here, we defined

$$I_1^{(m)}(a_*) := \int_{-\infty}^{\infty}d\tilde{k}'\int_{|\tilde{k}'|}^{\infty}d\tilde{\omega}'\frac{\tilde{\omega}'g'^{(m)}(\tilde{\omega}',\tilde{k}')}{e^{(\tilde{\omega}'-m\tilde{\Omega}'_\phi)/\tilde{T}'}-1}, \tag{4.22}$$

$$I_2^{(m)}(a_*) := \int_{-\infty}^{\infty}d\tilde{k}'\int_{|\tilde{k}'|}^{\infty}d\tilde{\omega}'\frac{mg'^{(m)}(\tilde{\omega}',\tilde{k}')}{e^{(\tilde{\omega}'-m\tilde{\Omega}'_\phi)/\tilde{T}'}-1}, \tag{4.23}$$

with $g'^{(m)}(\tilde{\omega}', \tilde{k}') = g^{(m)}(\tilde{\omega}, \tilde{k})$. In the same manner as Eq. (4.8), we normalized the quantities $\Omega'_\phi$ and $T' = \kappa'/2\pi$ of the unboosted system in Eq. (3.65) as $\tilde{\Omega}'_\phi := M_K \Omega'_\phi$ and $\tilde{T}' := M_K T'$. Their explicit formulas are

$$\tilde{\Omega}'_\phi = \frac{(1/2)a_*}{1+\sqrt{1-a_*^2}}, \qquad \tilde{T}' = \frac{(1/4\pi)\sqrt{1-a_*^2}}{1+\sqrt{1-a_*^2}}, \tag{4.24}$$

and depend only on $a_*$. Note that we used the fact that the integrals of terms proportional to $\tilde{k}'$ vanish because the greybody factor is an even function of $\tilde{k}'$ (see Eqs. (4.30) and (4.31) of the next subsection), and thus, such terms are odd functions of $\tilde{k}'$. From Eqs. (4.17)–(4.19) and Eq. (3.61), the equation for $a_*$ is derived as

$$-\frac{1}{a_*}\frac{da_*}{dt} = 3H(a_*)\frac{J_\psi^4}{M^8}, \tag{4.25}$$

where

$$H(a_*) := \frac{9\pi}{4}\frac{G(a_*)}{a_*} - F(a_*). \tag{4.26}$$

Therefore, the time evolution of a thin black ring by the Hawking radiation is determined by the equations for $M$, $J_\psi$ and $a_*$, that is, Eqs. (4.17), (4.18) and (4.25). The remaining work is to calculate the greybody factors and obtain $F(a_*)$ and $H(a_*)$ of Eqs. (4.20) and (4.26) numerically.

## 4.3 Greybody factor

In the following, we discuss the greybody factor for a massless scalar field in a boosted Kerr string spacetime. Substituting the ansatz (4.5) into the Klein-Gordon equation (4.1) in the background of the boosted Kerr string (3.57), we get the following angular and radial wave equations for $S_\ell^m(\theta)$ and $R(r)$ [28]:

$$0 = \frac{1}{\sin\theta}\partial_\theta\left(\sin\theta\partial_\theta S_\ell^m\right) + \left[a^2\left(\omega^2-k^2\right)\cos^2\theta - \frac{m^2}{\sin^2\theta} + \lambda_{\ell m}\right]S_\ell^m, \tag{4.27}$$

$$\begin{aligned} 0 = {} & \Delta\partial_r\left(\Delta\partial_r R\right) - \Delta\left[k^2r^2 + a^2\omega^2 - 2\omega ma\cosh\sigma + \lambda_{\ell m}\right]R \\ & + \Big[\left[\omega\left(r^2+a^2\right) - ma\cosh\sigma\right]^2 + 2M_K r\left(r^2+a^2\right)\cosh^2\sigma\left(\omega - k\tanh\sigma\right)^2 \\ & \quad - 2M_K r\left(r^2+a^2\right)\omega^2 - m^2a^2\sinh^2\sigma + 4kmaM_K r\sinh\sigma\Big]R, \end{aligned} \tag{4.28}$$

where $\lambda_{\ell m}$ is the separation constant which is determined as an eigenvalue of (4.27). For small $a^2\left(\omega^2-k^2\right)$, the eigenvalues associated with the spheroidal wave functions $S_\ell^m$ are $\lambda_{\ell m} = \ell\left(\ell+1\right) + \mathcal{O}\left(a^2\left(\omega^2-k^2\right)\right)$ [29].

As we mentioned in Sec. 4.1, the greybody factor is calculated as the absorption probability of the incoming waves of the corresponding mode. With the tortoise coordinate $r_*$ and a new wave function $u$ defined by

$$dr_* = \frac{r^2+a^2}{\Delta}dr, \qquad R = \frac{1}{\sqrt{r^2+a^2}}u, \tag{4.29}$$

the radial wave equation (4.28) can be rewritten as the following equation of Schrödinger type:

$$\left[\frac{d^2}{dr_*^2} + \omega'^2 - V(r)\right] u = 0, \tag{4.30}$$

where $V(r)$ is the effective potential

$$\begin{aligned} V(r) =& \frac{\Delta\left\{2M_K r(r^2-2a^2) + a^2(r^2+a^2)\right\}}{(r^2+a^2)^4} \\ &+ \frac{\Delta(\omega'^2 a^2 + \lambda_{\ell m} + k'^2 r^2) + 4m\omega' M_K a r - m^2 a^2}{(r^2+a^2)^2}. \end{aligned} \tag{4.31}$$

Here, the quantities in the unboosted frame, $\omega'$ and $k'$, were introduced in the same manner as Eq. (4.16). Note that Eqs. (4.30) and (4.31) have the same form as the equations for a massive scalar field with angular frequency $\omega'$ and mass $|k'|$ in a four-dimensional Kerr spacetime. As the boundary condition, we impose the ingoing condition at the horizon. Then, $u$ behaves as

$$u(r_*) \sim \begin{cases} e^{-i\omega'_+ r_*} & \text{at} \quad r \to r_+, \\ A_{in} e^{-i\omega'_\infty r_*} + A_{out} e^{i\omega'_\infty r_*} & \text{at} \quad r \to \infty. \end{cases} \tag{4.32}$$

Here $\omega'_+ := \omega' - m\Omega'_\phi$ and $\omega'_\infty := \sqrt{\omega'^2 - k'^2}$. The greybody factor is written as

$$\Gamma'_{\ell m}(\omega', k') = 1 - \left|\frac{A_{out}}{A_{in}}\right|^2, \tag{4.33}$$

which has to be evaluated numerically.

In this thesis, we perform numerical calculations of the greybody factor in the case of the Emparan-Reall black ring, i.e., $a = 0$. In this case, $S_\ell^m(\theta)e^{im\phi}$ becomes the spherical harmonic function $Y_{\ell m}(\theta, \phi)$ and the greybody factor is independent of $m$, and therefore, the calculation becomes much simpler compared to the case $a \neq 0$. We developed a code to calculate the greybody factor in this situation. The left and right panels of Fig. 7 show the behaviors of the greybody factors of the first three even $\ell$ numbers for $\tilde{k}' = 0$ and 0.6, respectively. Our result is in good agreement with the analytic approximate formula for low-frequency waves in Ref. [30] (see also [31, 32]).

Note that if we take the limit $\tilde{\omega}' \to \tilde{k}'$ for $\tilde{k}' \neq 0$, the greybody factor is expected to approach a nonzero finite value.[3] Obtaining these values by numerical calculation is rather difficult because the greybody factors have to be evaluated at a very distant position $r/M \gg 1/v'^2$ with $v' = \sqrt{1-(k'/\omega')^2}$. Although these values are left uncertain in our calculation, we have checked that the error caused by this uncertainty is small. For example, the error in $F(0)$ of Eq. (5.9) is smaller than 0.1%.

[3] This behavior has been claimed in Ref. [30] and we have also checked it using an analytic toy model.

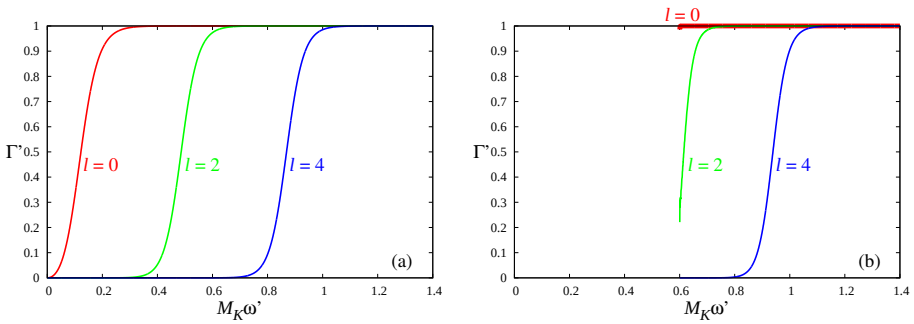


Figure 7: Greybody factors $\Gamma'$ as functions of $M_K\omega'$ for the modes $\ell = 0$, 2, and 4 in the case $a_* = 0$ for (a) $M_K k' = 0$ (left panel) and (b) $M_K k' = 0.6$ (right panel). In the right panel, the data for $M_K\omega' \geq 0.6005$ are plotted.

## 4.4 Absorption cross section

We check the validity of our numerical results in the previous subsection discussing an absorption cross section. Our numerical calculation was done for a thin Emparan-Reall black ring. In other words, we obtained the greybody factor for a massless scalar field in a five-dimensional boosted Schwarzschild string spacetime. Note that this is the same as the greybody factor for a massive scalar field in a four-dimensional Schwarzschild spacetime. Therefore, in this subsection, we discuss an absorption problem of the Schwarzschild black hole for massive scalar field with energy $\omega$ and mass $k$.

The relation between the partial absorption cross section $\sigma_\ell$ and the greybody factor $\Gamma_\ell$ is given by[30]

$$\sigma_\ell(\omega) = \frac{\pi}{\omega^2 v^2 r_s^2}(2\ell+1)\Gamma_\ell(\omega), \tag{4.34}$$

where $v^2 = 1 - k^2/\omega^2$ and $r_s$ is the horizon radius of the Schwarzschild black hole. Unruh derived the analytic expression of the low-energy partial absorption cross section for the massive scalar by matching the near-horizon radial solution and the asymptotic solution via the solution in the intermediate regime.

$$\sigma_\ell^{(\mathrm{Unruh})} = \frac{\pi}{\omega^2 v^2 r_s^2}(2\ell+1)\Gamma_\ell^{(\mathrm{Unruh})}, \tag{4.35}$$

$$\Gamma_\ell^{(\mathrm{Unruh})} = \frac{\pi(\ell!)^4 2^{2\ell+2}(1+v^2)\omega^{2\ell+3}v^{2\ell}r_s^{2\ell+3}}{(2\ell!)^4(2\ell+1)^2[1-\exp\{-\pi\omega(1+v^2)/v\}]}\prod_{s=1}^{\ell}\left[s^2+\left(\frac{\omega(1+v^2)}{2v}\right)^2\right].$$

The interesting result in Eq.(4.35) is the $S$-wave cross section($\ell = 0$), which is

$$\sigma_0^{(\mathrm{Unruh})} = \frac{(2\pi)^2(1+v^2)\omega r_s}{v^2[1-\exp\{-\pi\omega(1+v^2)/v\}]}. \tag{4.36}$$

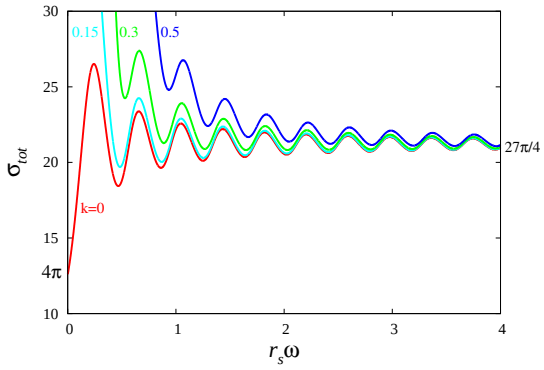


Figure 8: The total absorption cross sections as functions of $r_s\omega$ for $k = 0, 0.15, 0.3$ and $0.5$. The wiggly behaviour indicates that each partial absorption cross section has a peak at different energy scale. Regardless of mass the total absorption cross sections approach $27\pi/4$ at the high-energy limit. For $m = 0$, $\sigma_{tot}$ approaches $4\pi$ at the small $\omega$.

Taking $\omega \to 0$ limit and assuming $\omega \ll 1$, we have

$$\sigma_0^{(\mathrm{Unruh})} \sim 4\pi, \tag{4.37}$$

which equals to the horizon area. This is an universal property of the low-energy absorption cross section for massless scalar in black hole physics.

The total absorption cross section is given by

$$\sigma_{tot} = \sum_\ell \sigma_\ell. \tag{4.38}$$

$\sigma_{tot}$ has the wiggly pattern described by

$$\sigma_{tot}(\omega) = \frac{27\pi}{4} - \sqrt{2}\frac{\sin(\sqrt{2\pi}\pi\omega)}{\omega}, \tag{4.39}$$

because of the wave-black hole interaction in the effective potential [33]. This takes the limiting value $27\pi/4 \sim 21.2$ at large $\omega$ region. This also indicates that each partial cross section has a peak in a different value of $\omega$.

In Fig. 8, the total absorption cross sections are plotted as functions of $r_s\omega$ for four different masses $k = 0, 0.15, 0.3$ and $0.5$ (compare this figure with Fig.3 of Ref. [34]). For all value of $k$, the oscillatory patterns of $\sigma_{tot}$ appear and the total absorption cross sections approach $27\pi/4$ at large $\omega$ region. These results are consistent with Eq. (4.39). For the massless mode $k = 0$, $\sigma_{tot} \to 4\pi$ in the low energy limit $\omega \to 0$. This implies the behaviors of low-energy partial absorption cross sections as follows: in the low energy region, the partial cross section for $\ell = 0$ takes $4\pi$ as predicted in Unruh approximation, Eq. (4.37), while

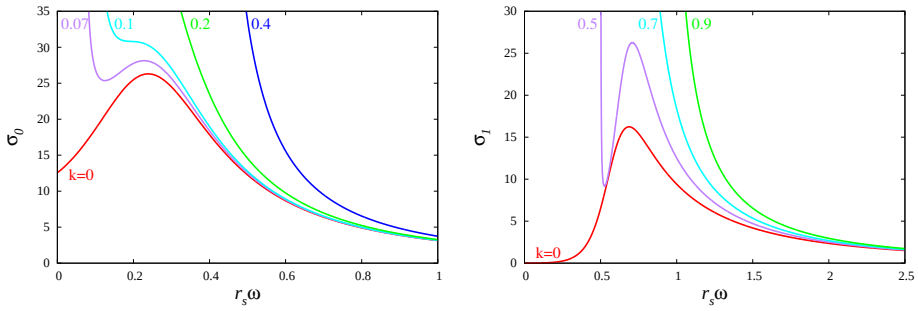


Figure 9: Partial absorption cross sections are plotted as functions of $r_s\omega$ for $\ell = 0$(left panel) and for $\ell = 1$(right panel). In the left panel, partial absorption cross sections $\sigma_0$ of $\ell = 0$ mode are shown for $k = 0, 0.07, 0.1, 0.2$ and $0.4$. $\sigma_0$ for the massless mode approaches $4\pi$ at the small $\omega$. In the right panel, partial absorption cross sections $\sigma_1$ of $\ell = 1$ mode are shown for $k = 0, 0.5, 0.7$ and $0.9$. $\sigma_1$ for the massless mode approaches zero at the small $\omega$.

the partial cross sections for $\ell > 0$ are zero. The implication can be confirmed in the next paragraph.

In Fig. 9, we plotted the partial absorption cross sections as functions of $r_s\omega$ for $\ell = 0$(left panel) and for $\ell = 1$(right panel). Compare these figures with Fig.7 of Ref. [34]. In the left panel, the partial absorption cross sections $\sigma_{\ell=0}$ are shown for $k = 0, 0.07, 0.1, 0.2$ and $0.4$. $\sigma_0$ for the massless mode approaches $4\pi$ at the small $\omega$. In the right panel, the partial absorption cross sections $\sigma_{\ell=1}$ are shown for $k = 0, 0.5, 0.7$ and $0.9$. $\sigma_1$ for the massless mode approaches zero at the small $\omega$. Therefore, in the low energy region, $\sigma_{\ell>0}$ approaches zero and only $\sigma_0$ contributes to the total absorption cross section. Moreover, the absorption cross sections of nonzero mass go to infinity in the sufficiently small $\omega$ region, which is independent of $\ell$. These are consistent with the behavior of the greybody factor discussed in the previous subsection. As shown in Fig. 7, while the greybody factor for massless mode approach zero if we take the limit $\omega \to k$, that for massive mode is still finite in the low energy limit. When we transform the greybody factor to the absorption cross section using Eq. (4.34), the massless and massive modes give $\sigma_\ell = 0$ and $\sigma_\ell \to \infty$, respectively.

# 5 Evolution by Evaporation

In this section, we discuss general features of the time evolution of the evaporating Pomeransky-Sen'kov black ring. Then, we focus attention to the case of the Emparan-Reall black ring, and derive semi-analytic solutions of the time evolution using the numerical results of the greybody factors.

## 5.1 Evolution of Pomeransky-Sen'kov black rings

First, we discuss general features that does not depend on the details of the greybody factor. From Eqs. (4.17) and (4.18), the following relation can be immediately found:

$$\frac{J_\psi^2}{M^3} = \text{const.} \tag{5.1}$$

From Eq. (3.62), this means that the thickness parameter $\lambda$ does not change,

$$\lambda(t) \equiv \lambda(0). \tag{5.2}$$

Therefore, a Pomeransky-Sen'kov black ring evaporates without changing the initial value of the nondimensional rotation parameter along $S^1$.

Next, let us assume $a_* > 0$ and consider how to solve the evolution equations for $a_*(t)$ and $M(t)$. Eliminating $M$ and $J_\psi$ from Eqs. (4.17) and (4.25) using Eq. (5.1), we obtain

$$\frac{d}{dt}\left(\frac{3a_* H(a_*)}{da_*/dt}\right) = 4F(a_*). \tag{5.3}$$

In principle, this equation can be solved at least numerically to yield $a_*(t)$ once $H(a_*)$ and $F(a_*)$ are specified. Then, from Eqs. (4.17) and (4.25), the time evolution of $M(t)$ is formally given by

$$M(t) = M(0) \exp\left[\frac{2}{3}\int_{a_*(0)}^{a_*(t)} \frac{F(a_*)}{a_* H(a_*)} da_*\right]. \tag{5.4}$$

We point out that the behavior of $H(a_*)$ is crucial for the evolution of $a_*$. This function is analogous to $h(a_*)$ of Ref. [14] where the evolution of a four-dimensional Kerr black hole was investigated: The value of $a_*$ increases (decreases) if $H(a_*)$ is negative (positive). If $H(a_*)$ crosses zero from negative to positive at some value $a_* = a_*^{(c)}$ similarly to Fig. 3 of Ref. [14], the black ring inevitably evolves to the state with $a_*^{(c)}$. Therefore, numerical calculation of $H(a_*)$ is very interesting, but is left for future work. In the present thesis, we only study what happens in the case of an Emparan-Reall black ring.

## 5.2 Evolution of Emparan-Reall black rings

In the case of the Emparan-Reall black ring, $J_\phi(t) \equiv 0$ and $a_* \equiv 0$, and Eqs. (4.17) and (4.18) can be solved analytically:

$$M(t) = M(0)\left(1 - 4F(0)\frac{J_\psi(0)^4}{M(0)^8} t\right)^{1/2}, \tag{5.5}$$

$$J_\psi(t) = J_\psi(0)\left(1 - 4F(0)\frac{J_\psi(0)^4}{M(0)^8}t\right)^{3/4}. \tag{5.6}$$

Therefore, our remaining task is to determine $F(0)$ numerically.

As discussed in Sec. 4.2, basically we have to calculate Eqs. (4.10), (4.22), and (4.20), and in those equations, the summation over $m$ was taken at the last step. But in the case of $a_* = 0$ considered here, it is better to take the summation with respect to $m$ in advance because the integrand does not depend on $m$. For this reason, we calculate summation of the greybody factors as

$$g'(\tilde{\omega}', \tilde{k}') := \sum_{\ell=0}^{\infty}\sum_{m=-\ell}^{\ell}\Gamma'_{\ell m}(\tilde{\omega}', \tilde{k}') = \sum_{\ell=0}^{\infty}(2\ell+1)\Gamma'_{\ell}(\tilde{\omega}', \tilde{k}'). \tag{5.7}$$

Then, $F(0)$ is given by

$$F(0) = \frac{3^7\pi^2}{2^3\sqrt{2}}I_1, \qquad I_1 := \int_{-\infty}^{\infty}d\tilde{k}'\int_{|\tilde{k}'|}^{\infty}d\tilde{\omega}'\frac{\tilde{\omega}'g'(\tilde{\omega}', \tilde{k}')}{e^{\tilde{\omega}'/\tilde{T}'} - 1}. \tag{5.8}$$

The integrations of $I_1$ were executed with the Simpson's method. The domain of integration of $I_1$ was made finite by discarding the region where the integrand is sufficiently small. We therefore set the upper limit of integration with respect to $\tilde{\omega}'$ to be 0.75. We took summation with respect to $\ell$ up to $\ell = 5$, because the contributions from the modes $\ell > 5$ turned out to be negligible. This is because the potential walls for $\ell > 5$ are so high that they reflect almost of all waves. In this manner, $F(0)$ is determined as

$$F(0) \simeq 0.239. \tag{5.9}$$

As a check, we compute $F(0)$ using the DeWitt approximation [41] in the next subsection. The two results agree well, and therefore, our numerical result is reliable.

As shown in Eq. (5.2), the nondimensional rotation parameter $J_\psi^2/M^3$ is held fixed throughout the evolution, and this also indicates the constancy of the thickness parameter $\lambda$. Because $a_* \equiv 0$, the Emparan-Reall black ring evaporates keeping similarity to its initial shape: The black ring at any time can be obtained by uniformly scaling its initial configuration. The scaling factor $C(t)$ can be found by deriving the time evolution of the ring radius $R$ as

$$C(t) := \frac{R(t)}{R(0)} = \left(1 - 4F(0)\frac{J_\psi(0)^4}{M(0)^8}t\right)^{1/4}. \tag{5.10}$$

The lifetime $t_{\rm LT}$ of a thin black ring with mass $M$ is

$$t_{\rm LT} \approx \left(\frac{27\pi\lambda}{4}\right)^2\left(\frac{M}{M_p}\right)^2 t_p, \tag{5.11}$$

where $M_p$ and $t_p$ are the Planck mass $(\hbar^2/G)^{1/3}$ and the Planck time $\hbar/M_pc^2$, respectively. The time scale is proportional to $M^2$, and this dependence on $M$ is

same as that of the five-dimensional Schwarzschild black hole. However, because of the prefactor $(27\pi\lambda/4)^2$, the lifetime of a thin black ring with $\lambda \lesssim 10^{-2}$ is much shorter than that of the five-dimensional Schwarzschild black hole with the same mass.

### 5.3 DeWitt approximation

In order to check the validity of our numerical result (5.9) of $F(0)$ in the case of the Emparan-Reall black ring, we compute this value in an approximate way. As the method of approximation, we adopt the DeWitt approximation [41] that was originally developed to evaluate the contribution of the greybody factor to the evaporation of a Schwarzschild black hole (see p. 394 of Ref. [35] for a review). In that study, the greybody factor was obtained by appropriately reinterpreting the capture condition of null geodesics. Although this approximation holds only for high-frequency regime in a strict sense, it gives a rather good result. In fact, the difference of the DeWitt approximation from the numerical result is $\approx 6\%$. Compare the formula of the mass-loss rate by the DeWitt approximation (Eq. (146) of Ref. [41]) and the numerical value reported in Ref. [14].

In the spacetime of a five-dimensional Schwarzschild string, a massless particle with momentum in the $z$ direction effectively behaves as a massive particle in a four-dimensional Schwarzschild spacetime. Therefore, as the first step, we study timelike geodesics in a four-dimensional Schwarzschild spacetime and derive the capture condition. Then, we translate it to the greybody factor for a massless scalar field in a spacetime of a Schwarzschild string. Using this result, we derive the value of $F(0)$ in the DeWitt approximation by performing the summation and integration in Eqs. (5.7) and (5.8).

The metric of a four-dimensional Schwarzschild spacetime is given by

$$ds^2 = -f(r)dt^2 + \frac{dr^2}{f(r)} + r^2(d\theta^2 + \sin^2\theta d\phi^2), \tag{5.12}$$

$$f(r) = 1 - \frac{2M_K}{r}. \tag{5.13}$$

This is the same metric as (2.11) if we take the mass parameter as $M_K = G_4 M_S$. The geodesic motion of a massive particle in the equatorial plane is governed by the following equations:

$$f(r)\dot{t} = e, \tag{5.14}$$

$$r^2\dot{\phi} = j, \tag{5.15}$$

$$-f(r)\dot{t}^2 + \frac{\dot{r}^2}{f(r)} + r^2\dot{\phi}^2 = -1. \tag{5.16}$$

Here, $e$ and $j$ indicate the energy and angular momentum per unit mass of the test particle, and dot ( $\dot{}$ ) denotes the derivative with respect to the particle's proper time $\tau$. Substituting Eqs. (5.14) and (5.15) into Eq. (5.16), we obtain

$$\dot{r}^2 + V(r) = e^2, \tag{5.17}$$

where

$$V(r) = \left(\frac{j^2}{r^2} + 1\right)\left(1 - \frac{2M_K}{r}\right). \tag{5.18}$$

Let us consider the situation where a test particle exists in the neighborhood of the horizon and moves toward outside (i.e. $\dot{r} > 0$). Denoting the peak value of $V(r)$ as $V_{\rm peak}$, the particle escapes to infinity if the condition $V_{\rm peak} < e^2$ is satisfied. Conversely, a particle with $V_{\rm peak} > e^2$ is reflected back to the black hole by the centrifugal barrier. After some calculation, the condition $V_{\rm peak} = e^2$ is shown to be equivalent to

$$j = e\sqrt{F(e)}M_K, \tag{5.19}$$

where

$$F(e) = \frac{27e^4 - 36e^2 + 8 + e(9e^2-8)^{3/2}}{2e^2(e^2-1)}. \tag{5.20}$$

Therefore, a particle escapes to infinity if $j < e\sqrt{F(e)}M_K$, and it is reflected back to the black hole if $j > e\sqrt{F(e)}M_K$. This condition is equivalent to the one obtained in Ref. [36]. Here, $\sqrt{F(e)}$ varies from 4 to $3\sqrt{3}$ as $e$ is increased from unity to infinity.

We use this result in order to approximate the greybody factor in the particle emission from the Schwarzschild string. Here, we choose the unboosted frame, and as done in Sec. 4.2, the quantities in this frame are indicated by prime ( $'$ ). Consider the emission of a quantum particle with mass $k'$, angular frequency $\omega'$, and angular quantum number $\ell$. Replacing $j \to \ell/k'$ and $e \to \omega'/k'$ in the capture condition derived above, the particle with $\ell \lesssim \omega'\sqrt{F(\omega'/k')}M_K$ escapes to infinity and that with $\ell \gtrsim \omega'\sqrt{F(\omega'/k')}M_K$ falls back to the horizon. Therefore, the greybody factor is approximated by

$$\Gamma'_{\ell m}(\tilde{\omega}', \tilde{k}') \approx \theta(\tilde{\omega}'\sqrt{F(\tilde{\omega}'/\tilde{k}')} - \ell), \tag{5.21}$$

where $\theta(u)$ denotes the Heaviside step function, and we introduced $\tilde{\omega}' = M_K\omega'$ and $\tilde{k}' = M_K k'$ in the same manner as Eq. (4.8). Note that in the massless particle limit, $\tilde{k}'/\tilde{\omega}' \to 0$, Eq. (5.21) becomes $\Gamma_{\ell mn} \approx \theta(3\sqrt{3}\tilde{\omega}' - \ell)$, and this agrees with the formula in the original DeWitt approximation [41].

Now, we evaluate the value of $F(0)$. The computation can be done with the formula given in Sec. 5.2. The quantity $g'(\tilde{\omega}', \tilde{k}')$ in Eq. (5.7) is

$$g'(\tilde{\omega}', \tilde{k}') = \sum_{\ell=0}^{\infty}(2\ell+1)\theta(\tilde{\omega}'\sqrt{F(\tilde{\omega}'/\tilde{k}')} - \ell) \approx \tilde{\omega}'^2 F(\tilde{\omega}'/\tilde{k}'). \tag{5.22}$$

Here, the summation over $\ell$ was changed by integration as done by DeWitt. Then, $F(0)$ can be calculated by substituting this formula into Eq. (5.8). It is convenient to introduce new variables $(x, y)$ by $x = \tilde{k}'/\tilde{\omega}'$ and $y = \tilde{\omega}'$, and in

these variables, analytic integration can be proceeded as

$$\begin{aligned} I_1 &= \int_0^\infty \frac{y^4 dy}{e^{8\pi y}-1} \int_{-1}^{1} dx F(1/|x|) \\ &= \frac{\zeta(5)}{4096\pi^5}\left[88 + 33\sqrt{2}\arcsin\left(\frac{2\sqrt{2}}{3}\right) - 3\log 3\right]. \end{aligned} \tag{5.23}$$

Substituting this result into Eq. (5.8), we obtain

$$F(0) \approx 1.40 \times 10^{-6} \tag{5.24}$$

This value is fairly close to our numerical value in Eq. (5.9): Similarly to the original DeWitt approximation for the Schwarzschild black hole, the approximate value is about 6% smaller compared to the numerical value. Therefore, the result of the DeWitt approximation supports the correctness of our numerical calculation.

# 6 Energy and angular spectra

In this section, we study the spectra of energy and angular momentum of radiated particles in the evaporation of a thin Emparan-Reall black ring.

## 6.1 Formulas for energy and angular spectra

For a thin Emparan-Reall black ring with $a_* = 0$, the emission rates of energy and angular momentum are given by Eqs. (4.13) and (4.14) with $dJ_\phi/dt = 0$. In Sec. 4.2, we simplified these formulas by performing the Lorentz transformation from $(\tilde{\omega}, \tilde{k})$ to $(\tilde{\omega}', \tilde{k}')$ through Eq. (4.16). Physically, this corresponds to the transformation from the boosted frame to the unboosted frame. Therefore, when we speak about the spectra, the two kinds of spectra can be considered: The spectra in the boosted frame (with respect to $\omega$) and those in the unboosted frame (with respect to $\omega'$). In this thesis, we prefer to analyze the spectra in the *boosted* frame, because the spectra in the boosted frame correspond to those for a distant observer at rest in the original black ring spacetime. For this reason, we rewrite Eqs. (4.13) and (4.14) in order to match them to our purpose here. Because the integrand does not depend on $m$ in the case of $a_* = 0$, we take summation with respect to $m$ in advance,

$$\sum_{m=-\infty}^{\infty} g^{(m)}(\tilde{\omega}, \tilde{k}) = \sum_{\ell=0}^{\infty} (2\ell + 1)\, \Gamma_\ell(\tilde{\omega}, \tilde{k}), \tag{6.1}$$

and change the order of integration with respect to $\tilde{\omega}$ and $\tilde{k}$ as

$$\int_{-\infty}^{\infty} d\tilde{k} \int_{|\tilde{k}|}^{\infty} d\tilde{\omega} = \int_{0}^{\infty} d\tilde{\omega} \int_{-\tilde{\omega}}^{\tilde{\omega}} d\tilde{k}. \tag{6.2}$$

Then, the formulas for the emission rates become

$$-\frac{dM}{dt} = \frac{R}{\sqrt{2}\pi M_K^3} \int_0^\infty d\tilde{\omega} \sum_{\ell=0}^{\infty} (2\ell + 1) \int_{-\tilde{\omega}}^{\tilde{\omega}} d\tilde{k} \frac{\tilde{\omega}\Gamma_\ell(\tilde{\omega}, \tilde{k})}{e^{(\tilde{\omega} - \tilde{k}V)/\tilde{T}} - 1}, \tag{6.3}$$

$$-\frac{dJ_\psi}{dt} = \frac{R^2}{\pi M_K^3} \int_0^\infty d\tilde{\omega} \sum_{\ell=0}^{\infty} (2\ell + 1) \int_{-\tilde{\omega}}^{\tilde{\omega}} d\tilde{k} \frac{\tilde{k}\Gamma_\ell(\tilde{\omega}, \tilde{k})}{e^{(\tilde{\omega} - \tilde{k}V)/\tilde{T}} - 1}. \tag{6.4}$$

Therefore, the energy and angular spectra are written as

$$-\frac{d^2M}{dtd\tilde{\omega}} = \frac{R}{\sqrt{2}\pi M_K^3} \frac{dI_M}{d\tilde{\omega}}, \qquad -\frac{d^2J_\psi}{dtd\tilde{\omega}} = \frac{R^2}{\pi M_K^3} \frac{dI_J}{d\tilde{\omega}}, \tag{6.5}$$

with the definitions

$$\frac{dI_M}{d\tilde{\omega}} := \sum_{\ell=0}^{\infty} (2\ell + 1) \int_{-\tilde{\omega}}^{\tilde{\omega}} d\tilde{k} \frac{\tilde{\omega}\Gamma_\ell(\tilde{\omega}, \tilde{k})}{e^{(\tilde{\omega} - \tilde{k}V)/\tilde{T}} - 1}, \tag{6.6}$$

$$\frac{dI_J}{d\tilde{\omega}} := \sum_{\ell=0}^{\infty} (2\ell+1) \int_{-\tilde{\omega}}^{\tilde{\omega}} d\tilde{k} \frac{\tilde{k}\Gamma_\ell(\tilde{\omega},\tilde{k})}{e^{(\tilde{\omega}-\tilde{k}V)/\tilde{T}}-1}. \tag{6.7}$$

The quantities $dI_M/d\tilde{\omega}$ and $dI_J/d\tilde{\omega}$ are interpreted as the rescaled energy and angular spectra.

We also would like to compare the energy spectrum of a thin black ring with that of a four-dimensional Schwarzschild black hole. The energy spectrum of evaporation of a four-dimensional Schwarzschild black hole with a mass $M_S = M_K/G_4$, where $G_4$ is the four-dimensional gravitational constant, is given by

$$-\frac{d^2M_S}{dtd\tilde{\omega}} = \frac{1}{M_K^2}\frac{dI_M^{(\mathrm{BH})}}{d\tilde{\omega}} \quad \text{with} \quad \frac{dI_M^{(\mathrm{BH})}}{d\tilde{\omega}} := \frac{1}{2\pi}\sum_{\ell=0}^{\infty}(2\ell+1)\frac{\tilde{\omega}\Gamma_\ell^{(\mathrm{BH})}(\tilde{\omega})}{e^{\tilde{\omega}/\tilde{T}'}-1}, \tag{6.8}$$

where $\Gamma_\ell^{(\mathrm{BH})}(\tilde{\omega})$ is the greybody factor for a massless scalar field in a four-dimensional Schwarzschild spacetime. Here, $dI_M^{(\mathrm{BH})}/d\tilde{\omega}$ is the rescaled energy spectrum. The trivial difference between the two energy emission rates (6.3) and (6.8) is that the black ring evaporation is different by a factor of $\sim R/M_K \sim 1/\lambda \gg 1$ compared to the four-dimensional black hole evaporation. This is because a large number of the Kaluza-Klein modes contribute to the black ring evaporation, while only massless modes contribute to the evaporation of a four-dimensional Schwarzschild black hole. In the following, we discuss the difference between the rescaled energy spectra $dI_M/d\tilde{\omega}$ and $dI_M^{(\mathrm{BH})}/d\tilde{\omega}$ apart from this trivial difference of $O(R/M_K)$.

## 6.2 Numerical results

Now, we present the numerical results.

### 6.2.1 Energy spectrum

Figure 10 shows the rescaled energy spectrum $dI_M/d\tilde{\omega}$ of emitted particles from a thin Emparan-Reall black ring as a function of $\tilde{\omega}$. The contributions from different quantum numbers $\ell = 0$, 1, and 2 are also plotted. only the $\ell = 0$ and 1 modes give the dominant contributions for the energy spectrum. The data for the higher multipole modes $\ell \geq 3$ are not plotted because they are tiny and invisible.

Let us discuss the feature of the energy spectrum of the black ring evaporation by comparing it with that of the evaporation of a four-dimensional Schwarzschild black hole. The numerical data of the energy spectra for a black ring and for a four-dimensional black hole are plotted in Fig. 11. First, we focus attention to the low-frequency region, $\tilde{\omega} \ll 1$. In this region, the energy spectrum for the black ring evaporation grows more slowly compared to that for the four-dimensional black hole as $\tilde{\omega}$ is increased. This feature can be explained by the approximate analysis as follows. In this region, the energy spectrum is approximately determined only by the $\ell = 0$ mode. Since the field equation in

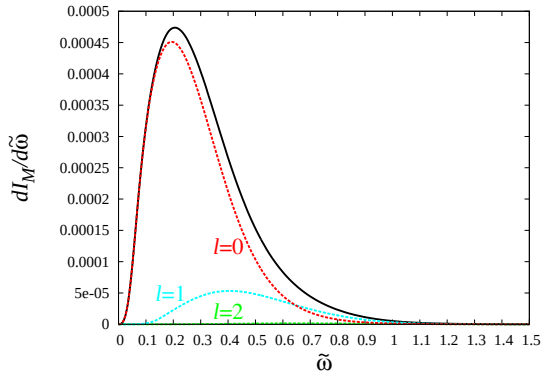


Figure 10: The rescaled energy spectrum $dI_M/d\tilde{\omega}$ as a function of $\tilde{\omega}$ together with the contributions of different quantum numbers $\ell = 0, 1$, and 2. This profile is proportional to the energy spectrum.

the unboosted frame is identical to the Klein-Gordon equation with mass $k'$, we can use Unruh's approximate formula [30] for the greybody factor,

$$\begin{aligned}\Gamma_0 &\approx \frac{32\pi(1+v'^2)\tilde{\omega}'^3}{1-\exp[-2\pi\tilde{\omega}'(1+v'^2)/v']} \\ &\approx 16\tilde{\omega}'\sqrt{\tilde{\omega}'^2-\tilde{k}'^2}+16\pi\tilde{\omega}'\left(2\tilde{\omega}'^2-\tilde{k}'^2\right)+\cdots,\end{aligned} \tag{6.9}$$

for the $\ell = 0$ mode, where $v' := \sqrt{1-\tilde{k}'^2/\tilde{\omega}'^2}$ is the velocity at infinity. Transforming this formula into the boosted frame and substituting it into Eq. (6.6), we find

$$\frac{dI_M}{d\tilde{\omega}} \approx \tilde{\omega}^3. \tag{6.10}$$

On the other hand, the approximate behavior of $dI_M^{(\mathrm{BH})}/d\tilde{\omega}$ for $\tilde{\omega} \ll 1$ for the four-dimensional Schwarzschild black hole is derived as

$$\frac{dI_M^{(\mathrm{BH})}}{d\tilde{\omega}} \approx \pi^{-2}\tilde{\omega}^2. \tag{6.11}$$

This explains the slower growth of the rescaled energy spectrum for the black ring compared to that for the four-dimensional black hole.

Next, we discuss the behavior in the high-frequency region $\tilde{\omega} \gg 1$. In this case, the greybody factor for a sufficiently small $\ell$ is approximately unity (see Fig. 7 and also Eq. (5.21) in Sec. 5.3), and therefore, the contribution from a mode with a sufficiently small $\ell$ is approximated as

$$\int_{-\tilde{\omega}}^{\tilde{\omega}} d\tilde{k}\frac{\tilde{\omega}\Gamma_\ell(\tilde{\omega},\tilde{k})}{e^{(\tilde{\omega}-\tilde{k}V)/\tilde{T}}-1} \approx \frac{\tilde{\omega}}{8\pi}e^{-8(\sqrt{2}-1)\pi\tilde{\omega}}. \tag{6.12}$$

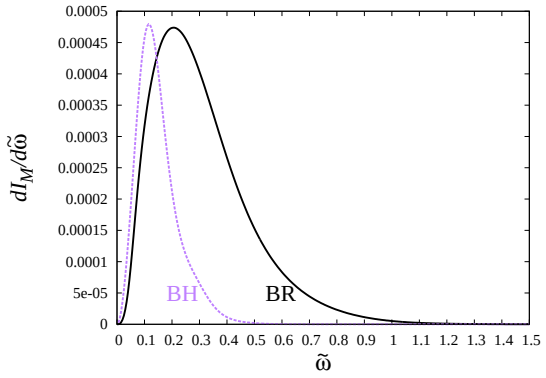


Figure 11: The rescaled energy spectra $dI_M/d\tilde{\omega}$ for a thin black ring and $dI_M^{(\mathrm{BH})}/d\tilde{\omega}$ for a four-dimensional Schwarzschild black hole as a function of $\tilde{\omega}$.

Since the number of the modes that contribute to the energy spectrum is $O(\tilde{\omega}^2)$, we have

$$\frac{dI_M}{d\tilde{\omega}} \sim \tilde{\omega}^3 e^{-8(\sqrt{2}-1)\pi\tilde{\omega}} \tag{6.13}$$

for $\tilde{\omega} \gg 1$ as an order estimate. On the other hand, for a four-dimensional Schwarzschild black hole, we have

$$\frac{dI_M^{(\mathrm{BH})}}{d\tilde{\omega}} \sim \tilde{\omega}^2 e^{-8\pi\tilde{\omega}}. \tag{6.14}$$

The remarkable difference of the black ring formula (6.13) from the black hole formula (6.14) is the presence of the factor $\sqrt{2}-1 \approx 0.414$ in the argument of the exponential function. Because of this factor, the energy spectrum for the black ring evaporation decays much more slowly than that for the black hole as $\tilde{\omega}$ is increased. We can also confirm this slower decay from our numerical data as shown in Fig. 11. The origin of this factor is the argument $(\tilde{\omega} - \tilde{k}V)/\tilde{T}$ in the exponential function of the denominator in the left-hand side of Eq. (6.12). In this formula, the momentum $\tilde{k}$ in the $z$ direction of the boosted black string spacetime enters like a chemical potential, and this "chemical potential term" enhances the emission rate of particles with positive momenta $\tilde{k} > 0$. From the viewpoint of the original black ring spacetime, more number of particles with positive angular momenta are emitted. Note that similar phenomena are observed in the evaporation of Kerr and Myers-Perry black holes [32, 37, 38, 39, 40]: The energy emission rate of a rotating black hole is also enhanced in the high-frequency regime compared to that of a Schwarzschild(-Tangherlini) black hole because of the effect of the chemical potential term.

The location of the peak has to be evaluated numerically. Our numerical result shows that the peak position is $\tilde{\omega} \simeq 0.21$ with the peak value $dI_M/d\tilde{\omega} = 4.73 \times 10^{-4}$. On the other hand, the peak position for the energy spectrum

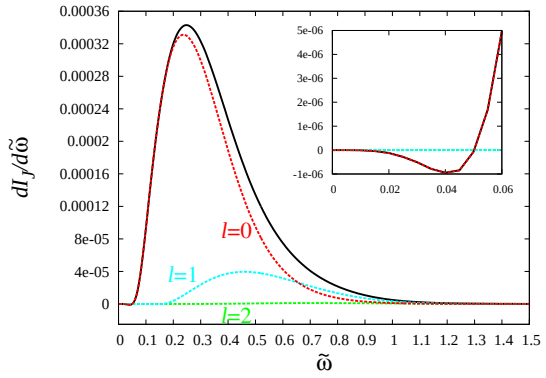


Figure 12: The rescaled angular spectrum $dI_J/d\tilde{\omega}$ as a function of $\tilde{\omega}$ together with the contributions of different quantum numbers $\ell = 0, 1$, and 2. The inset highlights the region $0 \leq \tilde{\omega} \leq 0.06$. This profile is proportional to the angular spectrum.

$dI_M/d\tilde{\omega}$ for a four-dimensional Schwarzschild black hole is $\tilde{\omega} \simeq 0.12$. The peak of $dI_M/d\tilde{\omega}$ is located at a higher frequency (in the unit of $M_K$) compared to that of $dI_M^{(\mathrm{BH})}/d\tilde{\omega}$. The difference in the peak positions comes from both the contribution from the Kaluza-Klein modes and the effect of the chemical potential term.

To summarize, the energy spectrum of emitted particles from a black ring shifts towards higher frequency domain compared to that from a four-dimensional black hole with the same value of $M_K$.

### 6.2.2 Angular spectrum

Now, we turn our attention to the angular spectrum. Figure 12 shows the rescaled angular spectrum $dI_J/d\tilde{\omega}$ as a function of $\tilde{\omega}$ together with the contributions of different quantum numbers $\ell = 0, 1$, and 2. The modes $\ell \geq 3$ are not plotted for the same reason as the rescaled energy spectrum. Again, the $\ell = 0$ and 1 modes give the dominant contributions to the angular spectrum.

First, we discuss the behavior in the low-frequency region. In this region, the spectrum is approximately determined only by the $\ell = 0$ mode. As we can see in the inset of Fig. 12, the rescaled angular spectrum is negative for $\tilde{\omega} \lesssim 0.05$. This behavior can be confirmed also from the approximate analysis. Substituting Unruh's approximate formula (6.9) for the greybody factor of the $\ell = 0$ mode into Eq. (6.7), we have

$$\frac{dI_J}{d\tilde{\omega}} \approx \left(\pi - \frac{8\sqrt{2}}{3}\right)\tilde{\omega}^4 \approx -0.630 \times \tilde{\omega}^4 \tag{6.15}$$

after some calculation. In discussing the reason for this negativity, there are two

important effects: The chemical potential term and the greybody factor. As discussed above, the chemical potential term enhances the emission rate of particles with positive $\tilde{k}$, and hence, tends to make the angular spectrum positive. On the other hand, for a fixed Lorentz invariant $\tilde{\omega}^2 - \tilde{k}^2$, the greybody factor is approximately proportional to the frequency $\tilde{\omega}'$ in the unboosted frame. Because $\tilde{\omega}' = \sqrt{2}\tilde{\omega} - \tilde{k}$, the positive momentum $\tilde{k}$ decreases the transmission probability to infinity for a given $\tilde{\omega}$. In other words, the relation $\Gamma(\tilde{\omega}, |\tilde{k}|) < \Gamma(\tilde{\omega}, -|\tilde{k}|)$ holds. The greybody factor suppresses the emission of particles with positive momenta $\tilde{k}$, and tends to make the angular spectrum negative. Therefore, the two effects compete with each other. At the leading order, the two effects cancel out and there is no $O(\tilde{\omega}^3)$ term in Eq. (6.15). At the subleading order, the effect of the greybody factor is stronger than the effect of the chemical potential, and this leads to the negative result of $O(\tilde{\omega}^4)$ in Eq. (6.15).

Next, we discuss the behavior in the high-frequency region $\tilde{\omega} \gg 1$. As done in the discussion on the energy spectrum, we approximate the greybody factor for a sufficiently small $\ell$ to be unity. Then, the contribution from a mode with a sufficiently small $\ell$ is approximated as

$$\int_{-\tilde{\omega}}^{\tilde{\omega}} d\tilde{k} \frac{\tilde{k}\Gamma_\ell(\tilde{\omega}, \tilde{k})}{e^{(\tilde{\omega} - \tilde{k}V)/\tilde{T}} - 1} \approx \frac{\tilde{\omega}}{8\pi} e^{-8(\sqrt{2}-1)\pi\tilde{\omega}}. \tag{6.16}$$

Since the number of the modes that contribute to the angular spectrum is $O(\tilde{\omega}^2)$, an order estimate gives

$$\frac{dI_J}{d\tilde{\omega}} \sim \tilde{\omega}^3 e^{-8(\sqrt{2}-1)\pi\tilde{\omega}}. \tag{6.17}$$

This is the same behavior as that of the energy spectrum, Eq. (6.13). The numerical result also shows the similarity in the behavior of $dI_M/d\tilde{\omega}$ and $dI_J/d\tilde{\omega}$ in the high-frequency region. Compare Figs. 10 and 12.

The peak position of the angular spectrum is numerically determined to be $\tilde{\omega} \simeq 0.25$ with $dI_J/d\tilde{\omega} \simeq 3.43 \times 10^{-4}$. This peak is located at a bit higher frequency than the peak location of the energy spectrum, and the peak values of $dI_M/d\tilde{\omega}$ and $dI_J/d\tilde{\omega}$ have the same order. To shortly summarize, a black ring emits positive angular momentum except for a small region $\tilde{\omega} \lesssim 0.05$, and the shape of the angular spectrum is similar to that of the energy spectrum.

## 6.3 Spectrum of a five-dimensional thin black string

Up to this point, we have studied the evaporation of an Emparan-Reall black ring in the thin-limit approximation. There, the evaporation of a black ring was approximated by that of a thin black string. Therefore, there is a close connection between the evaporation of a thin black ring and that of a thin black string. For this reason, our formalism and numerical code can be directly applied also to the evaporation of a thin Schwarzschild black string whose Schwarzschild radius $2M_K$ is much smaller than the compactification scale $L$ along the string direction. In this subsection, we study evaporation of a five-dimensional unboosted

thin Schwarzschild black string and present numerical results on detailed properties of the evaporation by comparing them with those of a four-dimensional Schwarzschild black hole. We also discuss the relation between these results and the evaporation of a thin black ring.

In this subsection, we use the unit $c = \hbar = G_4 = 1$ where $G_4$ is the four-dimensional gravitational constant.

### 6.3.1 Energy emission rate

We consider a five-dimensional Schwarzschild string with the metric

$$ds^2 = -f(r)dt^2 + \frac{dr^2}{f(r)} + r^2(d\theta^2 + \sin^2\theta d\phi^2) + dz^2, \qquad f(r) = 1 - \frac{2M_K}{r}. \tag{6.18}$$

Here, $z = 0$ and $L$ are identified and we consider the situation $L \gg M_K$. This black string is assumed to evaporate by emitting massless scalar particles in the five-dimensional spacetime. In the evaporation of a black string, the Kaluza-Klein modes with various values of momentum $k' = 2\pi n/L$ in the string direction contribute. Since these modes effectively behave as massive scalar fields in a four-dimensional spacetime, evaporation of a five-dimensional Schwarzschild string is identical to evaporation of a four-dimensional Schwarzschild black hole emitting scalar particles with various discrete masses. The energy emission rate of a black string is given by

$$-\frac{dM_K^{(\mathrm{BS})}}{dt} = \frac{1}{2\pi}\int_0^\infty d\omega' \sum_{\ell,m,n} \frac{\omega' \Gamma_{\ell mn}^{(\mathrm{BS})}(M_K\omega')}{e^{\omega'/T'} - 1}. \tag{6.19}$$

Since the black string is assumed to be thin, $L \gg M_K$, the summation over $n$ modes can be replaced by the integral with respect to $k'$:

$$\sum_n \to \int dn = \frac{L}{2\pi}\int dk'. \tag{6.20}$$

Then, the energy emission rate is

$$-\frac{dM_K^{(\mathrm{BS})}}{dt} = \frac{L}{4\pi^2 M_K^3} I_1^{(\mathrm{BS})}, \tag{6.21}$$

with

$$I_1^{(\mathrm{BS})} = \int_0^\infty d\tilde{\omega}' \frac{\tilde{\omega}'}{e^{\tilde{\omega}'/\tilde{T}'} - 1} \sum_{\ell=0}^\infty (2\ell+1) \int_{-\tilde{\omega}'}^{\tilde{\omega}'} d\tilde{k}' \Gamma_\ell^{(\mathrm{BS})}(\tilde{\omega}', \tilde{k}'). \tag{6.22}$$

Note that $I_1^{(\mathrm{BS})}$ is identical to $I_1$ of Eq. (5.8) that appeared in the analysis of evaporation of a thin black ring.

On the other hand, the energy emission rate for a Schwarzschild black hole emitting massless particles is

$$-\frac{dM_K^{(\mathrm{BH})}}{dt} = \frac{1}{2\pi}\int_0^\infty d\omega' \sum_{\ell,m} \frac{\omega' \Gamma_{\ell m}^{(\mathrm{BH})}(M_K\omega')}{e^{\omega'/T'}-1}. \tag{6.23}$$

Rewriting this formula with nondimensional quantities, we have

$$-\frac{dM_K^{(\mathrm{BH})}}{dt} = \frac{1}{2\pi M_K^2} I_1^{(\mathrm{BH})}, \tag{6.24}$$

with

$$I_1^{(\mathrm{BH})} = \int_0^\infty d\tilde{\omega}' \frac{\tilde{\omega}'}{e^{\tilde{\omega}'/\tilde{T}'}-1} \sum_{\ell=0}^{\infty} (2\ell+1)\Gamma_\ell^{(\mathrm{BH})}(\tilde{\omega}'). \tag{6.25}$$

Let us compare the two energy emission rates, Eqs. (6.21) and (6.24). The two integrals $I_1^{(\mathrm{BS})}$ and $I_1^{(\mathrm{BH})}$ have the same order, $I_1^{(\mathrm{BS})} \approx 1.25 \times 10^{-4}$ and $I_1^{(\mathrm{BH})} \approx 4.67 \times 10^{-4}$ (Here, our numerical result of $I_1^{(\mathrm{BH})}$ agrees with the value reported in Ref. [14]). Therefore, the energy emission rate of a black string is larger by a factor of $O(L/M_K)$ compared to that of a black hole. This is because more numbers of the Kaluza-Klein modes contribute to the emission as $L/M_K$ is increased. Therefore, in the Hawking radiation of a black string, as the string becomes thinner, its evaporation becomes faster compared to that of a Schwarzschild black hole whose mass is identical to the mass density of the black string.

### 6.3.2 Time evolution

Solving Eqs. (6.21) and (6.24), we have

$$M_K^{(\mathrm{BS})} = M_K(0)\left(1 - \frac{I_1^{(\mathrm{BS})} L}{\pi^2 M_K(0)^4} t\right)^{1/4}, \tag{6.26}$$

$$M_K^{(\mathrm{BH})} = M_K(0)\left(1 - \frac{3 I_1^{(\mathrm{BH})}}{2\pi M_K(0)^3} t\right)^{1/3}, \tag{6.27}$$

for a black string and a black hole, respectively. Because of the contribution of the massive modes in the black string case, the powers in these formulas are different from each other.

### 6.3.3 Energy spectrum

Let us focus attention to the energy spectrum. For this purpose, we introduce the "*effective greybody factor for the mode $\ell$*" for a black string with

$$\Gamma_\ell^{(\mathrm{eff})}(\tilde{\omega}') := \int_{-\tilde{\omega}'}^{\tilde{\omega}'} d\tilde{k}' \Gamma_\ell^{(\mathrm{BS})}(\tilde{\omega}', \tilde{k}'). \tag{6.28}$$

Then, the quantity $I_1^{(\mathrm{BS})}$ of Eq. (6.22) is expressed as

$$I_1^{(\mathrm{BS})} = \int_0^\infty d\tilde{\omega}' \frac{\tilde{\omega}'}{e^{\tilde{\omega}'/\tilde{T}'} - 1} \sum_{\ell=0}^{\infty} (2\ell+1)\Gamma_\ell^{(\mathrm{eff})}(\tilde{\omega}'). \tag{6.29}$$

Note that this formula is same as Eq. (6.25) except that $\Gamma_\ell^{(\mathrm{BH})}$ is replaced by $\Gamma_\ell^{(\mathrm{eff})}$. In addition, we introduce the "total effective greybody factor" by

$$\Gamma_{\mathrm{BS}}^{(\mathrm{eff})}(\tilde{\omega}') := \sum_{\ell=0}^{\infty} (2\ell+1)\Gamma_\ell^{(\mathrm{eff})}(\tilde{\omega}') \tag{6.30}$$

for a black string. The similar quantity is also introduced for a black hole as

$$\Gamma_{\mathrm{BH}}^{(\mathrm{eff})}(\tilde{\omega}') := \sum_{\ell=0}^{\infty} (2\ell+1)\Gamma_\ell^{(\mathrm{BH})}(\tilde{\omega}'). \tag{6.31}$$

In terms of these total effective greybody factors, the spectra of the quantities $I_1^{(\mathrm{BS})}$ and $I_1^{(\mathrm{BH})}$ with respect to $\tilde{\omega}'$ become

$$\frac{dI_1^{(\mathrm{BS})}}{d\tilde{\omega}'} = \frac{\tilde{\omega}'}{e^{\tilde{\omega}'/\tilde{T}'} - 1} \Gamma_{\mathrm{BS}}^{(\mathrm{eff})}(\tilde{\omega}'), \tag{6.32a}$$

$$\frac{dI_1^{(\mathrm{BH})}}{d\tilde{\omega}'} = \frac{\tilde{\omega}'}{e^{\tilde{\omega}'/\tilde{T}'} - 1} \Gamma_{\mathrm{BH}}^{(\mathrm{eff})}(\tilde{\omega}'). \tag{6.32b}$$

These quantities $dI_1^{(\mathrm{BS})}/d\tilde{\omega}'$ and $dI_1^{(\mathrm{BH})}/d\tilde{\omega}'$ are related to the energy spectra as

$$\frac{d^2E^{(\mathrm{BS})}}{dtd\tilde{\omega}'} = \frac{L}{4\pi^2 M_K^3} \frac{dI_1^{(\mathrm{BS})}}{d\tilde{\omega}'}, \tag{6.33a}$$

$$\frac{d^2E^{(\mathrm{BH})}}{dtd\tilde{\omega}'} = \frac{1}{2\pi M_K^2} \frac{dI_1^{(\mathrm{BH})}}{d\tilde{\omega}'}. \tag{6.33b}$$

Therefore, $dI_1^{(\mathrm{BS})}/d\tilde{\omega}'$ and $dI_1^{(\mathrm{BH})}/d\tilde{\omega}'$ can be called the rescaled energy spectra.

Figure 13 shows the effective greybody factors $\Gamma_\ell^{(\mathrm{eff})}$ for the mode $\ell$ as functions of $\tilde{\omega}'$ for $\ell = 0, ..., 5$. The greybody factor $\Gamma_\ell^{(\mathrm{BS})}(\tilde{\omega}', \tilde{k}')$ is approximately unity in the high frequency region $\tilde{\omega}' \gtrsim \ell/(3\sqrt{3})$ [see Eq. (5.21)], and therefore, $\Gamma_\ell^{(\mathrm{eff})}(\tilde{\omega}')$ behaves as

$$\Gamma_\ell^{(\mathrm{eff})}(\tilde{\omega}') \simeq \int_{-\tilde{\omega}'}^{\tilde{\omega}'} d\tilde{k}' = 2\tilde{\omega}'. \tag{6.34}$$

This behavior can be seen for $\ell = 0, 1$, and 2 in the domain of $\tilde{\omega}'$ shown in Fig. 13.

In Fig. 14, the total effective greybody factor $\Gamma_{\mathrm{BS}}^{(\mathrm{eff})}$ for a black string is plotted as a function of $\tilde{\omega}'$. The quantities $(2\ell+1)\Gamma_\ell^{(\mathrm{eff})}$ are also shown for the

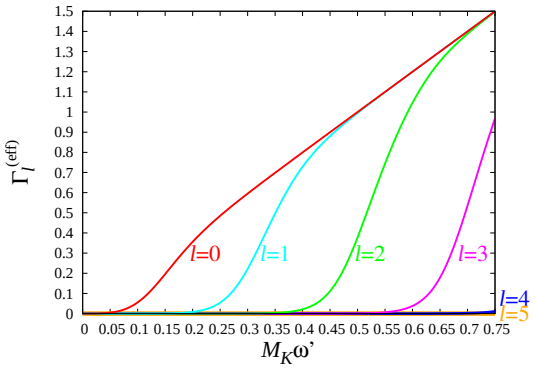


Figure 13: The effective greybody factors $\Gamma_\ell^{(\mathrm{eff})}$ for the mode $\ell$ introduced in Eq. (6.28) as functions of $M_K\omega'$ for the modes $\ell = 0, 1, 2, 3, 4$, and 5. In the high frequency region, $\Gamma_\ell^{(\mathrm{eff})}$ for the modes $\ell = 0, 1$, and 2 behave as $\approx 2M_K\omega'$.

first six $\ell$ modes. For comparison, we also plotted $\Gamma_{\mathrm{BH}}^{(\mathrm{eff})}$ for a black hole. The value of $\Gamma_{\mathrm{BH}}^{(\mathrm{eff})}$ is larger than that of $\Gamma_{\mathrm{BS}}^{(\mathrm{eff})}$ in the low frequency region, $\tilde{\omega}' \lesssim 0.55$. This is because the domain of integration of Eq. (6.28) becomes smaller as $\tilde{k}'$ is decreased. Also, the greybody factor is a monotonically decreasing function of $|\tilde{k}'|$ for a fixed $\tilde{\omega}'$. Conversely, in the high frequency region $\tilde{\omega}' \gtrsim 0.55$, we have $\Gamma_{\mathrm{BS}}^{(\mathrm{eff})} > \Gamma_{\mathrm{BH}}^{(\mathrm{eff})}$ reflecting the fact that domain of integration of Eq. (6.28) becomes larger than unity.

In Fig. 15, the rescaled energy spectrum $dI_1^{(\mathrm{BS})}/d\tilde{\omega}'$ for a black string is plotted as a function of $\tilde{\omega}'$ together with the contributions of different quantum numbers $\ell = 0, 1$, and 2. Although we plotted the modes $\ell = 3$, 4, and 5, they are tiny and invisible. For comparison, $dI_1^{(\mathrm{BH})}/d\tilde{\omega}'$ for a black hole is also plotted. Reflecting the results for $\Gamma_{\mathrm{BS}}^{(\mathrm{eff})}$ and $\Gamma_{\mathrm{BH}}^{(\mathrm{eff})}$, the value of $dI_1^{(\mathrm{BH})}/d\tilde{\omega}'$ is larger than that of $dI_1^{(\mathrm{BS})}/d\tilde{\omega}'$ in the low frequency region, $\tilde{\omega}' \lesssim 0.55$. The peak of $dI_1^{(\mathrm{BS})}/d\tilde{\omega}'$ is located at a slightly higher frequency compared to the peak location of $dI_1^{(\mathrm{BH})}/d\tilde{\omega}'$, and the decay of $dI_1^{(\mathrm{BS})}/d\tilde{\omega}'$ for the black string in the high frequency region is slower than $dI_1^{(\mathrm{BH})}/d\tilde{\omega}'$ for the black hole. Therefore, the energy spectrum of emitted particles from a black string shifts towards the higher frequencies compared to that from a black hole for a fixed $M_K$.

As in Sec. 6.2, we discuss the behaviors of the energy spectrum of the black string evaporation in the low and high frequency regions by comparing it with that of the evaporation of a four-dimensional Schwarzschild black hole. In the low-frequency region, $\tilde{\omega}' \ll 1$, the energy spectrum for the black string increases slowly compared to that for the Schwarzschild black hole as $\tilde{\omega}'$ is increased. Since the $\ell = 0$ mode dominates the energy spectrum in this region, using Unruh's approximation for greybody factor, (6.9), for the $\ell = 0$ mode, we have the

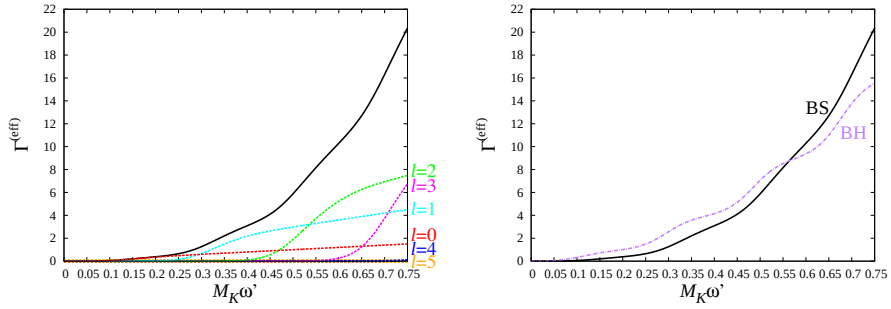


Figure 14: Left panel: The total effective greybody factor $\Gamma^{(\mathrm{eff})}_{\mathrm{BS}}$ for a black string introduced in Eq. (6.30) as a function of $M_K\omega'$ (solid line) together with the contributions from first six $\ell$ modes, $(2\ell+1)\Gamma^{(\mathrm{eff})}_{\ell}$. Right panel: Comparison between $\Gamma^{(\mathrm{eff})}_{\mathrm{BS}}$ and $\Gamma^{(\mathrm{eff})}_{\mathrm{BH}}$ (the solid line and the dash-dotted line, respectively). The value of $\Gamma^{(\mathrm{eff})}_{\mathrm{BH}}$ is larger than that of $\Gamma^{(\mathrm{eff})}_{\mathrm{BS}}$ in the low frequency region.

rescaled energy spectrum for the black string (6.32a) is approximated by

$$\frac{dI_1^{(\mathrm{BS})}}{d\tilde{\omega}'} \approx 2\tilde{\omega}'^3. \tag{6.35}$$

For the black string (6.32a), we have

$$\frac{dI_1^{(\mathrm{BH})}}{d\tilde{\omega}'} \approx \frac{2}{\pi}\tilde{\omega}'^2. \tag{6.36}$$

This explains the slower growth of the rescaled energy spectrum for the black string compared to that for the Schwarzschild black hole.

On the other hand, in the high-frequency region, $\tilde{\omega}' \gg 1$, the energy spectrum for the black string evaporation decays more slowly than that for the Schwarzschild black hole as $\tilde{\omega}'$ is increased. In this region, the greybody factor for a sufficiently small $\ell$ is approximately unity, and the summation with respect to $\ell$ is taken up to $\ell \sim O(\tilde{\omega}')$ (see Sec. 5.3). Using Eq. (6.34), we approximate the total effective greybody factor for the black string by

$$\Gamma^{(\mathrm{eff})}_{\mathrm{BS}}(\tilde{\omega}') \sim \tilde{\omega}'^2, \tag{6.37}$$

and for the black hole,

$$\Gamma^{(\mathrm{eff})}_{\mathrm{BH}}(\tilde{\omega}') \sim \tilde{\omega}'. \tag{6.38}$$

Therefore, in the high-frequency region, the rescaled energy spectrum for the black string behaves as

$$\frac{dI_M^{(\mathrm{BS})}}{d\tilde{\omega}'} \sim \tilde{\omega}'^3 e^{-8\pi\tilde{\omega}'}. \tag{6.39}$$

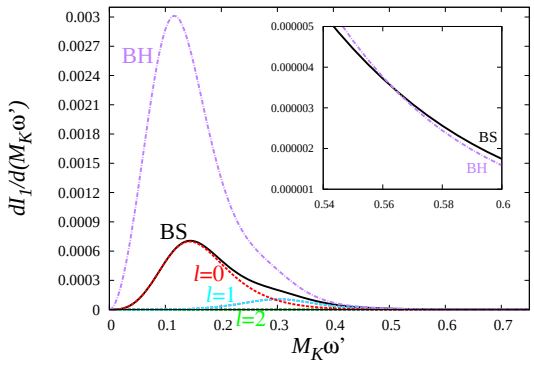


Figure 15: The rescaled energy spectrum $dI_1^{(\mathrm{BS})}/d\tilde{\omega}'$ of Eq. (6.32a) for a black string as a function of $M_K\omega'$ (the solid line) together with the contributions of different quantum numbers $\ell = 0, 1$, and 2. The contributions from the modes $\ell \geq 3$ are tiny and invisible. This profile is proportional to the energy spectrum. For comparison, $dI_1^{(\mathrm{BH})}/d\tilde{\omega}'$ for a black hole is also plotted (the dash-dotted line). The value of $dI_1^{(\mathrm{BH})}/d\tilde{\omega}'$ is larger than that of $dI_1^{(\mathrm{BS})}/d\tilde{\omega}'$ in the low frequency region. The inset highlights the region $0.54 \leq \tilde{\omega}' \leq 0.6$. The function $dI_1^{(\mathrm{BS})}/d\tilde{\omega}'$ decays more slowly compared to $dI_1^{(\mathrm{BH})}/d\tilde{\omega}'$ in the high frequency region.

For the black hole, we have

$$\frac{dI_M^{(\mathrm{BH})}}{d\tilde{\omega}'} \sim \tilde{\omega}'^2 e^{-8\pi\tilde{\omega}'}. \tag{6.40}$$

The difference in the power of $\tilde{\omega}'$ causes the slower decay of the rescaled energy spectrum for the black string compared to that for the Schwarzschild black hole.

### 6.3.4 Relation to the evaporation of a thin black ring

As already pointed out, the formula (6.22) of $I_1^{(\mathrm{BS})}$ for a thin black string is equivalent to $I_1$ of Eq. (5.8) that appeared in the analysis of a thin black ring. Similarly to $I_1^{(\mathrm{BS})}$ for a black string, the quantity $I_1$ gives the rescaled energy emission rate of a thin black ring as seen from Eqs. (5.8) and (4.17). For this reason, one might expect that the rescaled energy spectrum $dI_1^{(\mathrm{BS})}/d\tilde{\omega}'$ for a thin black string shown in Fig. 15 would also correspond to the rescaled energy spectrum $dI_1/d\tilde{\omega}'$ for a thin black ring. But we have to be careful in this reinterpretation.

In the case of a thin black ring, the function $dI_1/d\tilde{\omega}'$ is not proportional to the energy spectrum for observers at rest in an asymptotically flat region. This is because the energy spectrum for such observers has to be evaluated with

Eq. (4.13) where the frequency is given by $\tilde{\omega}$, not by $\tilde{\omega}'$. Originally, the transformation from $(\tilde{\omega}, \tilde{k})$ to $(\tilde{\omega}', \tilde{k}')$ was introduced in Eq. (4.16) in order to make calculations of Eqs. (4.13)–(4.15) easier. Physically, this transformation corresponds to the Lorentz transformation from the boosted frame to the unboosted frame. Therefore, $dI_1/d\tilde{\omega}'$ represents the rescaled energy spectrum for observers in the unboosted frame. From a viewpoint of the original black ring spacetime, the observers in the unboosted frame are moving in the $\psi$ direction with the angular velocity identical to the horizon angular velocity $\Omega_\psi$. Note that in order to avoid superluminal motion, such rotating observers have to stay in a region whose distance $d$ from the black ring horizon satisfies $M_K \ll d \ll R$.

# 7 Conclusion

In this thesis, we have studied the time evolution of evaporation of a thin black ring under the assumption that only a massless scalar field is emitted in the Hawking radiation. In order to separate the Klein-Gordon equation in the background of a black ring metric, we have considered the thin-limit approximation, where the black ring metric is approximated by the boosted Kerr string metric. Then, we have given a set of equations, Eqs. (4.17), (4.18) and (4.25), that determines the quasistationary evaporation of a thin Pomeransky-Sen'kov black ring. In this setup, a black ring evaporates without changing the thickness parameter $\lambda$. Also, we have analytically solved these equations in the case of an Emparan-Reall black ring and given its time evolution in Eqs. (5.5) and (5.6), with the factor $F(0) \simeq 0.239$ that has been determined by numerical calculation of the greybody factor. In the evaporation, the shape of the Emparan-Reall black ring keeps similarity to its initial configuration. The lifetime of a black ring is shorter by a factor of $O(\lambda^2)$ compared to a five-dimensional Schwarzschild black hole with the same initial mass.

We have also examined the energy and angular spectra of emitted particles in the evaporation of a thin Emparan-Reall black ring. Compared to the energy spectrum for a four-dimensional Schwarzschild black hole, the energy spectrum for a black ring shifts to high-frequency region. In particular, the decay rate of the black ring spectrum is slower than that for a four-dimensional black hole by a factor of $\sqrt{2}-1$ in the high-frequency region because of the effect of the "chemical potential" term. It has also been shown that the angular spectrum has a similar shape to that of the energy spectrum except in the low-frequency region $\tilde{\omega} \lesssim 0.05$ where the angular spectrum becomes negative due to the effect of the greybody factors.

As a closely connected system to a thin black ring, we applied our method also to the evaporation of a thin black string. In addition to the formulas for time evolution, we have given the numerical results on detailed properties of evaporation of a five-dimensional unboosted Schwarzschild black string by comparing them with those of a four-dimensional Schwarzschild black hole. Because of the contribution of the Kaluza-Klein modes, the energy emission rate of a black string is larger by a factor of $O(L/M_K)$ compared to that of a black hole. The energy spectrum of a black string shifts towards the higher frequencies compared to that of a black hole if we compare them fixing $M_K$. The energy spectrum of the Schwarzshild string is proportional to that of the thin Emparan-Reall black ring for observers rotating with the angular velocity identical to the horizon angular velocity $\Omega_\psi$.

As a future work, it is interesting to study the time evolution of a Pomeransky-Sen'kov black ring with nonvanishing rotational parameter $a_*$ along the $S^2$ direction. For this purpose, we have to calculate the functions $F(a_*)$ and $H(a_*)$ of Eqs. (4.20) and (4.26), and therefore, developing the code for computing the greybody factor of the boosted Kerr string is required. In addition, we are also interested in the time evolution of evaporation of a thin black ring in the case that massive and/or nonzero spin particles are emitted.

## Acknowledgments

I would like to express the deepest appreciation to Prof. Hideo Kodama, who is my supervisor and collaborator. He gave me precious advice for my research and supported my research activities. I would like to offer my special thanks to Hirotaka Yoshino. He is my collaborator and checked this manuscript. Without many fruitful discussions with him, my study discussed in the thesis cannot be accomplished. I also thanks to Kunihito Ioka, Kazunori Kohri, Akihiro Ishibashi. I had valuable opportunities to study cosmophysics in the seminars given by them. I also thank all other (ex-)members of the KEK theory center cosmophysics group. Especially, I am grateful to Masato Nozawa for checking this manuscript, Hajime Takami for useful advice on the thesis, and Yutaka Ohira for his advice on my numerical calculations. I would like to thank Sokendai students in the KEK theory center. I discussed with some of them personally, and studied with them in seminars. In particular, thanks to Hajime Goto, Keiki Saito, Hirotsugu Hayashi and Yoshihiko Oyama, who are(were) members of cosmophysics group, I had an enjoyable life in KEK.

Finally, I thank my family for their encouragement and mental supports.

# References


[1] B. Carter, Phys. Rev. Lett. **26**, 331 (1971).

[2] S. W. Hawking, Commun. Math. Phys. **25**, 152 (1972) .

[3] R. C. Myers and M. J. Perry, Annals Phys. **172**, 304 (1986).

[4] R. Emparan and H. S. Reall, Phys. Rev. Lett. **88**, 101101 (2002) [hep-th/0110260].

[5] H. Iguchi and T. Mishima, Phys. Rev. D **75**, 064018 (2007) [Erratum-ibid. D **78**, 069903 (2008)] [arXiv:hep-th/0701043].

[6] H. Elvang and P. Figueras, JHEP **0705**, 050 (2007) [arXiv:hep-th/0701035].

[7] H. Elvang and M. J. Rodriguez, JHEP **0804**, 045 (2008) [arXiv:0712.2425 [hep-th]].

[8] K. Izumi, Prog. Theor. Phys. **119**, 757 (2008) [arXiv:0712.0902 [hep-th]].

[9] R. Emparan and H. S. Reall, Living Rev. Rel. **11**, 6 (2008) [arXiv:0801.3471 [hep-th]].

[10] A. A. Pomeransky and R. A. Sen'kov, hep-th/0612005.

[11] S. W. Hawking, Commun. Math. Phys. **43**, 199 (1975).

[12] D. N. Page, Phys. Rev. D **13**, 198 (1976).

[13] D. N. Page, Phys. Rev. D **14**, 3260 (1976).

[14] C. M. Chambers, W. A. Hiscock and B. Taylor, Phys. Rev. Lett. **78**, 3249 (1997) [gr-qc/9703018].

[15] B. E. Taylor, C. M. Chambers and W. A. Hiscock, Phys. Rev. D **58**, 044012 (1998) [gr-qc/9801044].

[16] H. Nomura, S. Yoshida, M. Tanabe and K. -i. Maeda, Prog. Theor. Phys. **114**, 707 (2005). [hep-th/0502179].

[17] U. Miyamoto and K. Murata, Phys. Rev. D **77**, 024020 (2008) [arXiv:0705.3150 [hep-th]].

[18] B. Chen and W. He, Class. Quant. Grav. **25**, 135011 (2008) [arXiv:0705.2984 [gr-qc]].

[19] L. Zhao, Commun. Theor. Phys. **47**, 835 (2007) [hep-th/0602065].

[20] Q. -Q. Jiang, Phys. Rev. D **78**, 044009 (2008) [arXiv:0807.1358 [hep-th]].

[21] L. H. Ford, gr-qc/9707062.

[22] W. G. Unruh, Phys. Rev. D **10**, 3194 (1974).

[23] V. P. Frolov and D. Stojkovic, Phys. Rev. D **67**, 084004 (2003) [gr-qc/0211055].

[24] M. Nozawa and K. -i. Maeda, Phys. Rev. D **71**, 084028 (2005) [hep-th/0502166].

[25] Y. Chen, K. Hong and E. Teo, Phys. Rev. D **84**, 084030 (2011) [arXiv:1108.1849 [hep-th]].

[26] H. Elvang, R. Emparan and , JHEP **0311**, 035 (2003) [hep-th/0310008].

[27] Y. Morisawa, S. Tomizawa and Y. Yasui, Phys. Rev. D **77**, 064019 (2008) [arXiv:0710.4600 [hep-th]].

[28] O. J. C. Dias, Phys. Rev. D **73**, 124035 (2006) [hep-th/0602064].

[29] S. A. Teukolsky, Astrophys. J. **185**, 635 (1973).

[30] W. G. Unruh, Phys. Rev. D **14**, 3251 (1976).

[31] E. Jung, S. Kim and D. K. Park, JHEP **0409**, 005 (2004) [hep-th/0406117].

[32] P. Kanti and N. Pappas, Phys. Rev. D **82**, 024039 (2010) [arXiv:1003.5125 [hep-th]].

[33] N. G. Sanchez, Phys. Rev. D **16**, 937 (1977).

[34] E. Jung and D. K. Park, Class. Quant. Grav. **21**, 3717 (2004) [hep-th/0403251].

[35] V. P. Frolov and I. D. Novikov, *Black Hole Physics: Basic Concepts and New Developments*, (Kluwer Academic Publishers, Dordrecht and Boston, 1998).

[36] A. F. Zakharov, Soviet Astronomy **32**, 456 (1988).

[37] D. Ida, K. -y. Oda and S. C. Park, Phys. Rev. D **71**, 124039 (2005) [hep-th/0503052].

[38] C. M. Harris and P. Kanti, Phys. Lett. B **633**, 106 (2006) [hep-th/0503010].

[39] G. Duffy, C. Harris, P. Kanti and E. Winstanley, JHEP **0509**, 049 (2005) [hep-th/0507274].

[40] M. Casals, S. R. Dolan, P. Kanti and E. Winstanley, JHEP **0806**, 071 (2008) [arXiv:0801.4910 [hep-th]].

[41] B. S. DeWitt, Phys. Rept. **19**, 295 (1975).